ABSTRACT

In the spirit of the Air Force Office of Scientific Research's (AFOSR) initiative to promote university/industry collaborative research, a collaborative project entitled, *Numerical Flow Simulation for Complete Vehicle Configurations* has been executed by the National Science Foundation Engineering Research Center for Computational Field Simulation (NSF ERC) at Mississippi State University. The industrial participants include McDonnell Aircraft Company, McDonnell Douglas Research and Development Company and Teledyne Brown Engineering Company. The research and development activities of this effort are focused on the advancement of methodologies to increase the efficiency, quality and productivity of an overall CFD simulation associated with geometrically complex configurations. The progress realized in the aforestated development is presented in this report.

Progress concerning efforts designed to increase the efficiency and productivity of an overall CFD simulation process – from geometry definition to post processing of results as applied to complete aircraft configurations is presented. This progress has been brought about through enhancements in geometry processing, surface grid generation, grid refinement, grid adaptation, and domain decomposition strategies. The direct and inverse NURBS (Non Uniform Rational B–Spline) based surface representation is utilized in the development of algorithms for surface grid redistribution, automatic remapping, elliptic refinement and grid adaptation. The development of a procedure to identify "optimal" domain decomposition criteria by coupling the developed grid generation tools with various CFD analysis codes is initiated.

REPORT DOCUMENTATION PAGE

Form Approved
OMB No. 0704-0188

1. AGENCY USE ONLY (Leave blank)	2. REPORT DATE	3. REPORT TYPE AND DATES COVERED
	09-01-93	Final - 1 APR 90 - 31 MAR 93

4. TITLE AND SUBTITLE

Numerical Field Simulation around complete configuration

5. FUNDING NUMBERS

F49620-90-C-0027P0006

2307/AS

6. AUTHOR(S)

Bharat K. Soni

7. PERFORMING ORGANIZATION NAME(S) AND ADDRESS(ES)

NSF/Engineering Research Center
P.O. Box 6176
Mississippi State, MS 39762

MISSISSIPPI STATE UNIV.

8. PERFORMING ORGANIZATION REPORT NUMBER

9. SPONSORING/MONITORING AGENCY NAME(S) AND ADDRESS(ES)

Dr. Leonidas Sakell
AFOSR/NA
Directorate of Aerospace Sciences
Bldg 410
~~Bolling AFB, DC 20332-648~~

NA

10. SPONSORING/MONITORING AGENCY REPORT NUMBER

F49620-90-C-0027

11. SUPPLEMENTARY NOTES

12a. DISTRIBUTION/AVAILABILITY STATEMENT

Unclassified

12b. DISTRIBUTION CODE

Unli ited

13. ABSTRACT (Maximum 200 words)

In the spirit of the Air Force Office of Scientific Research's (AFOSR) initiative to promote university/industry collaborative research, a collaborative project entitled, *Numerical Flow Simulation for Complete Vehicle Configurations* has been executed by the National Science Foundation Engineering Research Center for Computational Field Simulation (NSF ERC) at Mississippi State University. The industrial participants include McDonnell Aircraft Company, McDonnell Douglas Research and Development Company and Teledyne Brown Engineering Company. The research and development activities of this effort are focused on the advancement of methodologies to increase the efficiency, quality and productivity of an overall CFD simulation associated with geometrically complex configurations. The progress realized in the aforestated development is presented in this report.

Progress concerning efforts designed to increase the efficiency and productivity of an overall CFD simulation process – from geometry definition to post processing of results as applied to complete aircraft configurations is presented. This progress has been brought about through enhancements in geometry processing, surface grid generation, grid refinement, grid adaptation, and domain decomposition strategies. The direct and inverse NURBS (Non Uniform Rational B-Spline) based surface representation is utilized in the development of algorithms for surface grid redistribution, automatic remapping, elliptic refinement and grid adaptation. The development of a procedure to identify "optimal" domain decomposition criteria by coupling the developed grid generation tools with various CFD analysis codes is initiated.

14. SUBJECT TERMS

Computational Fluid Dynamics, Grid Generation, Grid Adaptation, Domain Decomposition

15. NUMBER OF PAGES

75

16. PRICE CODE

17. SECURITY CLASSIFICATION OF REPORT	18. SECURITY CLASSIFICATION OF THIS PAGE	19. SECURITY CLASSIFICATION OF ABSTRACT	20. LIMITATION OF ABSTRACT
U	U	U	

DISCLAIMER NOTICE

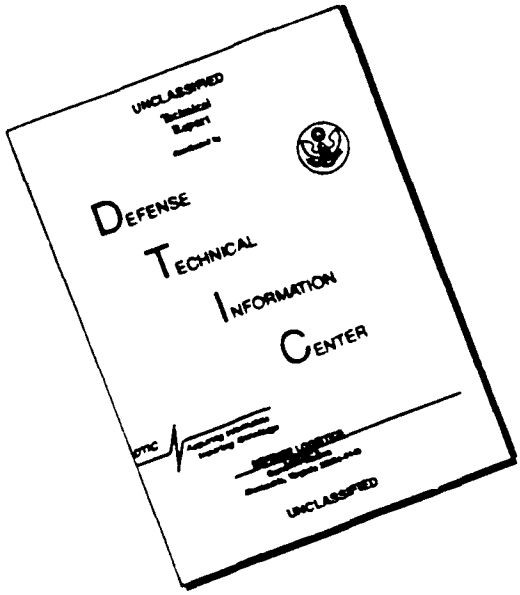

THIS DOCUMENT IS BEST QUALITY AVAILABLE. THE COPY FURNISHED TO DTIC CONTAINED A SIGNIFICANT NUMBER OF PAGES WHICH DO NOT REPRODUCE LEGIBLY.

TABLE OF CONTENTS

Appendix A.7 .....

"Interpolation Code for Post-Processing Comparison and Analysis: User's Guide", Prepared by Paul E. Craft, Graduate Student.

Appendix A.8 .....

"GENIE ++, EAGLEView and TIGER: General and Special Purpose Graphically Interactive Grid Systems", AIAA-92-0071, *30th AIAA Aerospace Sciences Meeting,* Reno, NV, January 1992.

Appendix A.9 .....

"Grid Generation: A Key Thrust Area at The NSF Engineering Research Center for Computational Field Simulation", *Proceedings of the Third International Conference in Numerical Grid Generation in CFD,* Barcelona, Spain, September 1991.

Appendix A.10 .....

PARC Code Summary

Appendix A.11 .....

EAGLE Code Summary

Appendix A.12 .....

Grid Optimization

Appendix A.13 .....

Grid Adaptation

Appendix A.14 .....

Zone Subset Grid

TECHNICAL PROJECT REPORT

Project

Numerical Flow Simulations for Complete Vehicle Configurations

Submitted By

Dr. Bharat K. Soni, Principle Investigator
Associate Professor
NSF Engineering Research Center for
Computational Field Simulation
Department of Aerospace Engineering
Mississippi State University
Mississippi State, MS 39762

601-325-8278
601-325-7692 Fax

Submitted To

Dr. Leonidas Sakell, Program Manager
Directorate of Aerospace Sciences
AFOSR/NA
Bolling Air Force Base
Washington, DC 20322-6448

Period of Performance

April 1, 1990 - March 31, 1993

BACKGROUND

Mississippi State University (MSU), in collaboration with members of the National Science Foundation Engineering Research Center for Computational Field Simulation at Mississippi State University (MSU) has established a collaborative research program funded by AFOSR, McDonnell Aircraft Company (McAir), and McDonnell Douglas Research & Development (MDRL) and Teledyne Brown Engineering (TBE) Corporation.

The broad–based objective of this research project is to improve understanding of fluid phenomena associated with complex three–dimensional full (e. g. complete aircraft) configurations under various physical environments. In particular, the research emphasis is place on:

- Grid generation associated with grids about complete aircraft configurations
  a. Efficiency and Economy
  b. Block/Zone Strategies and Methodologies
  c. Adaptive Gridding
- Solution algorithms
  a. Block/Zone Strategies
  b. Solution Adaptation
  c. Parallel Processing
- Training of CFD applications specialists
  a. University/Industry personnel

The key element of this project is the technology transfer providing one–on–one interactions between university personnel and scientists from various aerospace industries. This program is a three–year collaborative effort. This report summarizes the accomplishments and algorithms developed during the execution of this overall broad–based research program.

INTRODUCTION

There is little doubt that the use of various types of mathematical modeling has significantly enhanced almost every aspect of hardware design, including not only evaluation of basic concepts, but also in the prototyping post–production stages. The manner in which modeling affects design processes has been shown to reduce cost, risk, and enhance the overall final product. A particular type of modeling which has increasingly come into play over the past several years is now commonly referred to as computational fluid dynamics (CFD), which involves numerically solving a set of partial differential equations over some spatial and temporal domain. The use of CFD has been shown to be particularly well–suited to the aerospace industry (Ref. 1). CFD has also been extensively utilized in the ground testing of many aerospace configurations ranging from subscale aircraft models to full–scale missiles, to full–scale turbine and rocket engines (Ref. 2–3).

To use CFD in the analysis of a particular fluid flow problem, several things must either exist or be created and must function as a complete system to be useful: (1). generation of a "computational

grid", where the spatial region of interest is split up, or discretized, into many smaller regions, (2). execution of a software package (sometimes referred to as a "flow solver"), which is a set of instructions making up the numerical algorithm with which the particular set of partial differential equations are solved, (3) execution of post–processing software designed to allow the rendering of large amounts of digital information into graphical or analog depictions of a particular flowfield phenomena, (4) a computer powerful enough (in terms of speed and memory size) to execute the flowfield solver in a practical amount of time, and (5) personnel skilled in the use of this software and hardware and in the interpretation of computed results.

In the spirit of AFOSR's initiative to promote university/industry collaborative research, the project entitled, "Numerical Flow Simulation for Complete Vehicle Configuration" has been launched involving McDonnell Aircraft Company, McDonnell Douglas Research and Development Company, and Teledyne Brown Engineering Company and the NSF Engineering Research Center for Computational Field Simulation at Mississippi State University. The research and development activities of this effort is focused on the advancement of full Navier–Stokes flow simulation algorithms to predict more accurately and efficiently the flow phenomena involving complex configurations. In particular, the research emphasis is placed on: surface/geometry generation, domain decomposition, strategies, solution adaptive grids, grid refinement, parallel processing, and numerical algorithms for simulation of various physical environments associated with complete vehicle configurations.

OBJECTIVES

The broad–based objective of this research project is to provide a forum through which university and industrial researchers can jointly pursue research and development pertinent to the simulation of fluid flowfields (steady and unsteady) about complete flight vehicles over a wide range of flight conditions. Upon completion, this research will significantly reduce the "response time" for addressing complex CAD applications and will increase the quality of simulation through the improvement of numerical algorithms, surface rendering and grid generation schemes, and the manner in which graphical techniques are used to interpret computed solutions. Specifically, research focused upon advancing the current state of knowledge regarding the following items is being conducted:

a. Grid Generation
   - Surface/Geometry Generation
   - Grid Optimization
   - Domain Decomposition Strategies
   - Adaptive Gridding

b. Flowfield Solution Algorithms
   - Parallel Processing
   - Block Interface Treatment
   - Solution Adaptive Techniques

c. Training of CFD Applications Specialists

d. Applications: The present approach is centered around performing computations about the complete F15 Figher Aircraft.

TECHNICAL APPROACH

The primary objective is to improve all facets of the CFD technology associated with efficient and "optimal" simulation of complete flight vehicle configurations. Numerical geometry grid generation is considered the most labor intensive part of any CFD application. In fact, at present it can take significantly more labor time to construct a CFD grid than it does to execute the flow field simulation code on the grid or to analyze results. Also, 80%–90% of the grid generation labor time is usually spent on geometry processing. Therefore, initial emphasis is placed on grid generation enhancments with the objective of increasing efficiency, quality, and productivity. To this end, a candidate complete aircraft configuration was selected. Three distinct geometric descriptions of the same fighter aircraft with distinct refrence and scaling criteria were obtained in the form of: (i) a CAD/CAM geometry description, (ii) a set of forty–nine sculptured surfaces and (iii) a volume grid around a wing/body/vertical–horizonal tail. These configurations were studied and analyzed to investigate algorithm development which could expedite the grid generation process. In this respect, graphical user interactions, CAD interface, and automatic/interactive multi–block interface construction have already been explored in the general purpose grid systems: GRAPEVine, EAGLEView, GRIDGEN, ICEM, IGG, and others. However, there exists a need to develop methodologies to redistribute, refine and automatically remap surface grids while maintaining the fidelity of the geometrical description of the original surfaces along with robust control functions for elliptic generation and grid adaptive schemes. In order to explore all research issues associated with the simulations; the following technology development must be undertaken:

TA.1. Surface Grid Generation

Develop/adapt methodologies to manipulate and define surface grids associated with the complete geometry. These surface grids must satisfy the requirements associated with the structured physical to computational mapping pertinent to domain decomposition strategies under consideration.

TA.2. Grid Construction

Develop/adapt techniques to optimize 2D/3D grids associated with the complex geometries under consideration. This optimization must result in efficiency and economy of the overall grid generation process.

TA.3. Grid Adaptation

Develop/adapt grid adaptive procedure and validate with respect to complex configurations.

TA.4. Flowfield Simulations

Adapt flowfield solution codes and simulate flowfields involving various physical environments. This must include increasingly complex configurations such as F15e and cruise missile geometries.

TA.5. Domain Decomposition

Develop domain decomposition strategies. This is accomplished as follows:

a. Generate a multiblock grid around a configuration under consideration. Identify block boundaries/surfaces strictly on the basis of geometrical characteristics.

b. Optimize boundaries/surfaces mesh for improved orthogonality and smoothness and hence refine the grid using the grid optimization process.

c. Simulate multiblock flowfield utilizing the blocked grid.

d. Analyze and compare these solutions in order to evaluate "optimal" placement of block boundaries/surfaces. This will be accomplished on the basis of the equidistribution law.

e. Regenerate optimized grid and repeat steps c through d until optimal placement of boundaries/surfaces is achieved.

TA.6. Parallel Processing

Develop parallel processing methodologies for the single block and multiblock environment being studied.

TA.7. Validation

Validate solution results in comparison with available test data and analyze the pay–off from the enhanced technology.

The computer programs EAGLEView (Ref. 4–6) and GENIE (Ref. 7–9) are utilized for accomplishing grid generation and the codes PARC3D (Ref. 10) and EAGLE (Ref. 11–12) are used for flowfield simulations. PARC3D is based on the finite difference approximate factorization scheme, however, EAGLE is based on finite volume Roe's upwind scheme.

All research activities should be performed collaboratively between MSU researchers and industrial partners.

ACCOMPLISHMENTS

First Year's Accomplishments

During the first year, the F15e geometry was acquired from Wright Patterson AFB and General Dynamics. The grid generation and flowfield simulations on a single block configuration involving wing/fuselage with inlet merged with fuselage (no flow through inlet) were performed. These simulations were performed with $M_\infty = 1.5$, $\alpha = 0°$ utilizing finite difference and finite volume codes. The following enhancements were made in grid technology:

Surface Generation

The sculptured cubic B–spline surface representation in direct and inverse forms was developed for surface grid generation.

Grid Optimization

A grid optimization based on the best characteristics of algebraic and elliptic generation system was developed and coded for the two–dimensional applications.

Grid Adaptation

A two–dimensional grid adaptative algorithm based on the algebraic technique and quick elliptic optimization algorithm was initiated.

Zone Subset Grid

The EAGLEView grid generation system was enhanced for subset elliptic grid generation. This was accomplished by allowing higher order continuity at the subset boundary interface.

Second Year's Accomplishments

During the second year, the following tasks were performed:

Surface Generation

The sculptured cubic B–spline surface representation in direct and inverse form is extended to the general Non–Uniform Rational B–spline representation.

Grid Optimization

A Hermite transfinite interpolation algorithm with automatic evaluations of slopes and proper twist vectors is developed. A grid optimization algorithm developed during first year is extended to three–dimensional applications. A novel approach to evaluate control functions for elliptic generation system is developed.

Grid Adaptation

A two–dimensional grid adaptive algorithm is developed based on the equidistribution principle utilizing the best characteristics of algebraic or elliptic general system. A weight function is formulated using the Boolean sum of using various physical characteristics and adaptation. A code is completely validated and transferred on to Teledyne Brown Engineering.

GENIE Enhancements

In order to interpret, manipulate and define the F15e CAD geometry, various curve/surface manipulation routines are developed in GENIE. These routines are added to the development of CAGI (Ref. 13) code.

Domain Decomposition

To evaluate criteria for domain decomposition strategies a grid–flowfield simulation around an isolated wing is performed.

Interpolation/Search Algorithm

An interpolation code for post–processing comparison and analysis is developed.

Third Year's Accomplishments

Redistribution and Remapping Algorithms

The NURBS representation for surfaces is utilized to redistribute geometrically complex surfaces with desired point distribution criteria. An algorithm to automatically remap surface grids is developed. The remapping algorithm allows the automatic generation of surface grids containing trimmed subsurfaces, gaps, and independent grids (e.g. wing–body intersection on the body). The body surface grid can be automatically generated by blending the intersected wing part as the part of the grid.

Grid Optimization

The surface grid optimization based on the Hermite interpolation parametric space associated with NURBS surface is developed. The elliptic generation system with the control functions developed during the second year have been extended for the surface grid refinement.

Grid Adaptation

The algebraic grid adaptive scheme has been extended to three dimensions. The redistribution scheme along with weight function based on a Boolean sum of flow characteristics has been enhanced for surface–by–surface grid adaptation in the desired direction (or combination of directions e.g. I, J, or J, K or I, K, or I, J, K). Various computational examples of practical interest were exercised using this grid adaptation scheme.

Complete F15 Configurations & Domain Decomposition Strategies

The grid generation process associated with the complete F15 aircraft configuration has been completed. The work on the simulation and determination of "optimal" placement of zonal interfaces is on–going or continuing.

Applications

Three different F15e grid configurations have been utilized to establish a baseline computational capability and to evaluate enhancements made in the grid/simulation methodology. These configurations are:

i. Wing/fuselage: Single block and four-block configuration - 580,000 grid points. (Figure 1a-d).

ii. Vertical-horizontal tail/wing/fuselage: Five block configuration (Figure 2a-b) using c-grid on the fuselage. This grid was acquired from McDonnell Aircraft Company.

iii. Vertical-horizontal tail/wing/fuselage: Five block configuration using H-O grid on the fuselage (Figure 3).

iv. Complete configuration body/inlet/nozzle (Figures 4-20).

In the wing/fuselage configurations, approximately 580,000 grid points were used for single block (173 x 42 x 80 grid). Approximately 2.2 million grid points were used in the C–H tail/wing/fuselage configuration.

The purpose of this research was to produce a detailed three–dimensional volume grid of the full–configuration F–15 EAGLE. The grid was constructured using the grid generation package GENIE^{++}, an algebraic grid system developed by Dr. B. K. Soni at the National Science Foundation Engineering Research Center located at Mississippi State University.

The original geometry definition for the F–15 was supplied in the form of 49 surfaces, each describing a distinct part of the aircraft. These surfaces varied in dimension and orientation with respect to the plane of symmetry. Using GENIE^{++}, the surfaces were refined and fit together in order to maintain continuity along grid lines. The refinement was accomplished using the Akima spline routine found in GENIE^{++}. This spline scheme allowed for manipulation of the surfaces while maintaining the integrity of the geometry definition. Once the grid of the surface geometry was completed and considered of acceptable quality, development of the volume grid was begun.

The first surface grid was a wing/body/tail combination. This grid was a highly accurate representation of the fuselage, wing, and vertical and horizontal tails, but did not attempt to model the inlet. Instead, the fuselage was smoothly molded into the wing, simplifying the geometry. This grid contained 5 blocks and was a C–type grid. Numerous solutions were performed on this grid, and one of these is included in the accompanying figures.

The size of the final volume grid was 81 x 141 60, or 685, 260 grid points, with the i–direction wrapping around the body, the j–direction streamwise, and the k–direction normal to the surface. The surface grid included the fuselage, the inlet, the nozzle, and a flow–through chamber connecting the inlet to the nozzle. In order to properly execute a solution algorithm on the grid, the volume grid was broken into 5 blocks. Accurate modeling of the inlet and nozzle regions was considered of high priority for this grid, and considerable effort was invested to achieve this goal. Numerous pictures of the final surface and volume grids are included.

Future plans include completing the present surface grid by adding the wing and the horizontal and vertical tails. The domain decomposition of this grid may prove to be a difficult process due to the complexity of the geometry. Also, accurate simulation of the flow through the inlet/nozzle combination will be a strong test for the solution algorithm.

A comparative study is made between a finite difference versus a finite volume code. The aforementioned configuration was simulated on the parallel processor in collaboration with BRL scientists.

University–Industry Collaboration

The broad–based objective of the present collaborative project is to provide a forum through which university and industrial researchers can jointly pursue research and development pertinent to the simulation of fluid flowfields about complete flight vehicles over a wide range of flight conditions. To this end, during this year, the following activities were performed:

- Paul Adams, a MSU graduate student in Aerospace Engineering spend three semesters (one semester during the first year and two semesters during the second year) at McDonnell Douglas Research and Development Laboratory (MDRL) as an intern. He graduated in the Fall of 1992 with a master's thesis entitled, *Decomposition Strategies for A Multiblock Time Dependent Grid About A Helicopter Rotor/Fuselage Configuration*. His work was supported and funded by MDRL. The experience gained in this study will be applied to complete F15 simulations.

- Paul Craft, an MSU graduate student in Aerospace Engineering spent a semester at MDRL as a summer intern. He is working on the Domain Decomposition Strategies and Interpolation/Search techniques applicable to multiblock configurations. He will present his Master's thesis in December 1993.

- Various trips to St. Louis were made by MSU researchers. In particular, five-three day trips (on average) per year, to St. Louis were made by MSU researchers. This has facilitated the close working relationship between MSU, McDonnell Aircraft Company (McAir), and MDRL engineers.

  Two graduate students and one undergraduate student visited St. Louis with faculty members. Mr. Bruce Vu, who is a Ph.D. student, is pursuing his research in Domain Decomposition Strategies on F15e configurations.

- Three trips, per year, to Huntsville, Alabama, were made by MSU faculty and graduate students. Mr. Jiann-Cherng Yang has completed a Ph.D. in computational engineering with research emphasis on grid adaptation. MSU researchers worked very closely with researchers at Teledyne Brown Engineering regarding their requirements.

- MDRL, McAir and Teledyne Brown Engineering researchers made two trips to MSU. These trips were organized in conjunction with NSF Engineering Research Center for Computational Field Simulation industrial programs and collaborative project related schedule.

- Two trips to the U. S. Army Ballistic Research Laboratory (BRL) were made by MSU researchers. A collaborative effort has progressed between BRL and MSU in the area of parallel processing. Two trips were made by BRL researchers to MSU.

- The work associated with grid quality analysis was conducted due to contractual arrangement between McAir and MSU. This analysis has been utilized in grid generation associated with multiblock strategies for F15 complete configuration.

- The work on helicopter configurations has been conducted due to contracted arrangements between MDRL and MSU. The challenge of gridding helicopter blade rotation in a multiblock environment has made a singificant contribution in the development of grid generation techniques associated with rotating machinery.

- The work on adaptive gridding is conducted due to contractual arrangement between Teledyne Brown Engineering and MSU. The adaptive algorithm, especially in three dimensions, will be directly applicable to F15 flow field simulation and domain decomposition strategies.

The university–industry collaboration is working out very well for both industry and the university. The facility at the Engineering Research Center at Mississippi State University provides an excellent environment for industrial visitors as well as for this overall collaboration. This collaboration has been proven to be very beneficial to participating students. Three Ph.D. students, two masters students, and four undergraduate students have participated in this overall effort.

THEORETICAL DEVELOPMENT

NURBS Surface Representation

The Non–Uniform Rational B–spline curve and surface representation (Ref. 14–15) is developed in direct and inverse formulation for redistributing complex surface grids. In general a NURBS curve is expressed as

$$G(t) = \frac{\sum_{i=0}^{K} W(i)\ P(i)\ b_i(t)}{\sum_{i=0}^{K} W(i)\ b_i\ (t)} \qquad (1)$$

where the notation is interpreted as follows:

The $W(i)$ are the weights (positive real numbers).

The $P(i)$ are the control points (points in R^3).

The b_i are the $B-$ spline basis functions.

A NURBS surface (3–D) can be expressed parametrically in the form (Ref. 14):

$$G\ (s,t) = \frac{\sum_{i=0}^{K1} \sum_{j=0}^{K2} W(i,\ j)\ P(i,\ j)\, b_i(s)\ b_j\ (t)}{\sum_{i=0}^{K1} \sum_{j=0}^{K2} W(i,\ j)\, b_i\ (s)\ b_j\ (t)} \qquad (2)$$

where

The $W(i,j)$ are the weights (positive real numbers).

The $P(i,\ j)$ are the control points (points in R^3).

The b_i are the B–spline basis functions of degree *M1* determined by the know sequence *S (–M1), . . ., S (N1 + M1).* The b_j are the B–spline basis functions of degree M1 determined by the know sequence *T (–M2), . . . , T (N2 + M2).* Here, $N1 = K1 - M1 + 1$ and $N2 = K2 - M2 + 1$.

The surface itself is parametrized for $U(0) \le s \le U(1)$ and for $V(0) \le t \le V(1)$ where $S(0) \le U(0) < U(1) \le S(N1)$ and $T(0) \le V(0) < V(1) \le T(N2)$.

For a given curve with a set of data points: $x_0, x_1, \ldots, x_L$, we can find the control points as follows in (Ref. 14):

Define the chord length parameterization as

$$\frac{\Delta_i}{\Delta_{i+1}} = \frac{\| \Delta x_i \|}{\| \Delta x_{i+1} \|} \qquad \text{where } \Delta_i = x_{i+1} - x_i$$

The control points $d_0, d_1, \ldots, d_L$ can be obtained by solving the matrix

$$\begin{bmatrix} 1 & & & & \\ \alpha_1 & \beta_1 & \gamma_1 & & \\ & \ddots & \ddots & \ddots & \\ & & \alpha_{L-1} & \beta_{L-1} & \gamma_{L-1} \\ & & & & 1 \end{bmatrix} \begin{bmatrix} d_0 \\ d_1 \\ \vdots \\ d_{L-1} \\ d_L \end{bmatrix} = \begin{bmatrix} r_0 \\ r_1 \\ \vdots \\ r_{L-1} \\ r_L \end{bmatrix} \tag{3}$$

where

$$r_0 = b_1,$$

$$r_i = (\Delta_{i-1} + \Delta_i)\, x_i,$$

$$r_L = b_{3L-1},$$

$$\alpha_i = \frac{\Delta_i^2}{\Delta_{i-2} + \Delta_{i-1} + \Delta_i}, \tag{4}$$

$$\beta_i = \frac{\Delta_i (\Delta_{i-2} + \Delta_{i-1})}{\Delta_{i-2} + \Delta_{i-1} + \Delta_i} + \frac{\Delta_{i-1} (\Delta_i + \Delta_{i+1})}{\Delta_{i-1} + \Delta_i + \Delta_{i+1}},$$

$$\gamma_i = \frac{\Delta_i^2}{\Delta_{i-1} + \Delta_i + \Delta_{i+1}}.$$

and then set

$$d_{-1} = x_0, \quad d_{L-1} = x_L$$

The control points of the surface are determined using the tensor product formula associated with both v, s, and t parametrics.

Algebraic Surface Grid Optimization

Let $r = (x, y, z)$ be the physical coordinates and (ξ, η) denote the computational space for the surface. Let $r(s, t) = (x(s, t), y(s, t), z(s, t))$ be the NURBS parametric representation of the surface with (s, t) as the parametric space. Now as demonstration in the Figure 21, there exists a one to one relation–

ship between physical space, parametric space and computational space. Using this argument a surface grid optimization algorithm is developed in view of optimizing orthogonality.

For orthogonality

$$r_\xi \cdot r_\eta = 0 \quad \textit{is required}$$

i.e.

$$(r_s s_\xi + r_t t_\xi) \cdot (r_s s_\eta + r_t t_\eta) = 0$$

i.e.

$$(r_s \cdot r_s) s_\xi s_\eta + (r_s \cdot r_t)(s_\xi t_\eta + t_\xi s_\eta) + (r_t \cdot r_t) t_\xi t_\eta = 0 \qquad (6)$$

and also

$$r_\eta \cdot r_\eta = d^2$$

represents the desired distance space in η direction

i.e.

$$(r_s s_\eta + r_t t_\eta) \cdot (r_s s_\eta + r_t t_\eta) = d^2 \qquad (7)$$

i.e.

$$(r_s \cdot r_s) s_\eta^2 + 2(r_s \cdot r_t)(s_\eta t_\eta) + r_t \cdot r_t t_\eta^2 = d^2 \qquad (8)$$

Now the parametric space is formulated as the normalized arc length as presented in Figure 22. On the boundary $\eta = 1$ and $\eta = \eta_{max}$, $t_\xi = 0$ and therefore equation (6) results in

$$(r_s \cdot r_s) s_\xi s_\eta + (r_s \cdot r_t) s_\xi t_\eta = 0 \qquad (9)$$

Since s_ξ can be computed using finite difference formulations on the boundaries $\eta = 1$ and $\eta = \eta_{max}$, the equations (8) and (9) can be solved for s_η and t_η.

Similarily, the equations

can be solved for s_ξ and t_ξ on $\xi = 1$ and $\xi = \xi_{max}$ boundaries. This information can then be utilized to complete Hermite transfinite interpolation on the parametric space and the surface grid points can be re-evaluated on the redistributed parametric space.

$$r_\xi \cdot r_\eta = 0$$

and

$$r_\xi \cdot r_\xi = (\textit{desired distance } \eta \ \xi \textit{ direction})^2$$

The computational example of this technique is presented in the Figure 23 a–f. As it can be seen in the Figure 23 the optimized surface grid is orthogonal near boundaries.

Robust Hermite Transfinite Interpolation Scheme

The Transfinite Interpolation Method (Ref. 4–9, 16) is a widely used grid generation technique. It is based on a Boolean sum of the one dimensional parametric interpolation schemes. The utilization of Hermite cubic representation in grid generation is attractive because of the control over slopes near boundary/boundary surface. However, the evaluation of these slopes is extremely crucial. The quality of the resulting grid is highly influenced by the magnitude of the slopes and the twist vectors (cross derivatives). An algorithm to evaluate slopes and twist vectors is developed. Let $r = (x, y, z)$ and $\Omega = (\xi, \eta, \text{and } \varsigma)$ denote the physical and computational space respectively. Then for Hermite interpolation in ξ direction the vector $\underline{r}_\varsigma$ should be obtained at $\xi = \xi_{min}$ and $\xi = \xi_{max}$ surfaces. The following equations are utilized in evaluation of $\underline{r}_\xi$:

$$\begin{aligned} \underline{r}_\xi \cdot \underline{r}_\eta &= 0 \\ \underline{r}_\xi \cdot \underline{r}_\zeta &= 0 \\ \underline{r}_\xi \cdot (\underline{r}_\eta \times \underline{r}_\zeta) &= V \end{aligned} \tag{10}$$

Where the desired cell volume is calculated from the initial linear TFI grid. The twist vectors are calculated using the following equations.

$$\begin{aligned} (\underline{r}_\xi \cdot \underline{r}_\eta)_\eta &= 0 \\ (\underline{r}_\xi \cdot \underline{r}_\zeta)_\eta &= 0 \\ (\underline{r}_\xi \cdot (\underline{r}_\eta \times \underline{r}_\zeta))_\eta &= V_\eta \end{aligned} \tag{11}$$

and

$$\begin{aligned} (\underline{r}_\xi \cdot \underline{r}_\eta)_\zeta &= 0 \\ (\underline{r}_\xi \cdot \underline{r}_\zeta)_\zeta &= 0 \\ (\underline{r}_\xi \cdot (\underline{r}_\eta \times \underline{r}_\zeta))_\zeta &= V_\zeta \end{aligned} \tag{12}$$

ELLIPTIC REFINEMENT

Let $\underline{r} = (x_1, x_2, x_3)$ and $\underline{\Omega} = (\xi_1, \xi_2, \xi_3)$ denote physical and computational space respectively. Define covariant and contravariant vectors (Ref. 48) as follows:

$$\underline{a}_i = \text{covariant vectors } \underline{r}_{\xi^i} \quad (i = 1,2,3);$$

$$\underline{a}^i = \text{contravariant vectors } \underline{\nabla}\xi^i \, (i = 1,2,3)$$

$$g_{ij} = \underline{a}_i \cdot \underline{a}_j = g_{ji} \quad (i = 1,2,3), \quad (j = 1,2,3)$$

$$g^{ij} = \underline{a}^i \cdot \underline{a}^j = g^{ji} \quad (i = 1,2,3), \quad (j = 1,2,3)$$

$$g = \det | g_{ij} | = [\underline{a}_1 \cdot (\underline{a}_2 \times \underline{a}_3)]^2$$

Now

$$(g_{ij})_{\xi^k} \equiv (\text{derivative of } g_{ij} \text{ with respect to } \xi^k)$$

$$\equiv \underline{r}_{\xi^i\xi^k} \cdot \underline{r}_{\xi^j} + \underline{r}_{\xi^i} \cdot \underline{r}_{\xi^j\xi^k} \cdot \cdot \cdot \cdot \cdot \tag{13}$$

$$i = 1,2,3; \; j = 1,2,3; \; \text{and} \; k = 1,2,3.$$

Using (13), the following statement can be obtained

$$\underline{r}_{\xi^i\xi^j} \cdot \underline{r}_{\xi^k} = \frac{(g_{ik})_{\xi^j} - (g_{ij})_{\xi^k} + (g_{jk})_{\xi^i}}{2} \tag{14}$$

$$i = 1,2,3; \; j = 1,2,3; \; k = 1,2,3;$$

Consider a three dimensional elliptic grid generation system

$$\sum_{i=1}^{3} \sum_{j=1}^{3} g^{ij} \underline{r}_{\xi^i\xi^j} + \sum_{k=1}^{3} \phi_k \underline{r}_{\xi^k} = 0 \tag{15}$$

where

$$g^{i\ell} = \frac{1}{g} (g_{jm} g_{km} - g_{jn} g_{kn})$$

$$i = 1,2,3; \; j = 1,2,3$$

(i, j, k) and (ℓ, m, n) cyclic

Our analysis for evaluation of ϕ_k is as follows:

In order to evaluate the forcing functions ϕ_k, $k = 1,2,3$, usual practice is to write (15) as

$$\sum_{i=1}^{3} \sum_{j=1}^{3} g^{ij} \underline{r}_{\xi\xi}^{ij} \cdot \underline{r}_{\xi^q} + \sum_{k=1}^{3} \phi_k \underline{r}_{\xi^k} \cdot \underline{r}_{\xi^q} = 0 \tag{16}$$

$$q = 1,2,3$$

Using (13), Equation (15) can be rewritten as follows:

$$\sum_{i=1}^{3} \sum_{j=1}^{3} g^{ij} (g_{iq})_{\xi^j} + \sum_{k=1}^{3} \phi_k g_{kq}$$

$$- \sum_{i=1}^{3} \sum_{j=1}^{3} g^{ij} (\underline{r}_{\xi^i} \cdot \underline{r}_{\xi^j \xi^q}) = 0 \tag{17}$$

$$q = 1,2,3$$

Observe that, using (13)–(15), Equation (17) can be written in terms of metric terms and their derivatives. Also

$$g_{ii} = \underline{r}_{\xi^i} \cdot \underline{r}_{\xi^i} = \| r_{\xi^i} \|^2$$

represent an increment of arc length on a coordinate line along lines which ξ^i varies and

$$g_{ij} = \underline{r}_{\xi^i} \cdot \underline{r}_{\xi^j} = \| r_{\xi^i} \| \cdot \| r_{\xi^j} \| \cdot \cos\theta, \; i \neq j$$

represent measure of orthogonality between grid lines along which ξ^i and ξ^j varies. These quantities can be evaluated if the desired increment in the arc length and the desired angles between grid lines are known.

Looking at the "precise control of spacing" property of the algebraic grid (Ref. 49), the quantities "g_{ij}" can be evaluated from the well–defined algebraic grid, and using

$$g_{ij} = \left(\sqrt{g_{ii}} \right) \left(\sqrt{g_{jj}} \right) (\cos\theta)$$

where θ is the desired angle between ξ^i, ξ^j grid lines, the quantities g_{ij}, $i \neq j$ can be evaluated. Once all g_{ij}'s are known, the Equation (17) can be solved for the forcing functions ϕ_k, $k = 1,2,3$. In particular when orthogonality is assumed i.e., $\theta = 90°$ or $g_{ij} = 0$ for $i \neq j$, then ϕ_k, $k = 1,2,3$ can be formulated as

$$\hat{\phi}_k = \frac{1}{2} \frac{d}{d\xi^k} \left(\ln \frac{g_{kk}}{g_{ii}\, g_{jj}} \right), \quad (i,\ j,\ k) \quad cyclic \tag{18}$$

$$k = 1, 2, 3$$

where

$$\hat{\phi}_k = - \frac{g\, \phi_k}{g_{ii}\, g_{jj}}, \quad (i,\ j,\ k,) \quad cyclic \tag{19}$$

$$i, j, k = 1, 2, 3$$

we assume that $g_{ii} \neq 0$ for $i = 1, 2, 3$

An application of these control functions result in a smooth/nearly orthogonal grid in fewer iterations (3–5) of the elliptic solver. Two examples demonstrating the application of these control functions (3 iterations) on surfaces involving smooth and sharp concave and convex regions are presented in Figure 24a–f and Figure 25a–d. It can be observed that the elliptic grid is smooth and near orthogonal in both cases.

These control functions are applied in surface/volume grid refinement. The surface elliptic system is obtained by transforming Eq. (15) into the parametric form (Ref. 49). The two-dimensional parametric space (distribution mesh) is refined and then surface coordinates are evaluated from NURBS representation. The detailed mathematical description for surface grid optimization is provided as follows:

QUASI-TWO-DIMENSIONAL ELLIPTIC SYSTEM

Assumptions

1. The surface is represented as a coordinate surface

$$\zeta = constant$$

2. The ξ and η lines are perpendicular to the ς lines

$$i.\ e.\ g_{13} = 0 \quad \text{and} \quad g_{23} = 0$$

3. The principal curvature of the ς lines vanish on the surface

$$g_{22}\,(r_{\xi\xi} - \phi r_\xi) - 2g_{12}\, r_{\xi\eta} + g_{11}\,(r_{\eta\eta} - \phi\, r_\eta) = \varkappa\, |\, r_\xi \times r_\eta\, |\, (r_\xi \times r_\eta)$$

where

$$\varkappa = \frac{g_{22} r_{\xi\xi} \cdot (r_\xi \times r_\eta) - 2g_{12} r_{\xi\eta} \cdot (r_\xi \times r_\eta) + g_{11} r_{\eta\eta} \cdot (r_\xi \times r_\eta)}{|\, r_\xi \times r_\eta\, |^3}$$

By the chain rule for differentiation,

$$r_\xi = r_s s_\xi + r_t t_\xi$$

$$r_\eta = r_s s_\eta + r_t t_\eta$$

$$r_{\xi\xi} = r_{ss} s_\xi^2 + 2 r_{st} s_\xi t_\xi + r_{tt} t_\xi^2 + r_s s_{\xi\xi} + r_t t_{\xi\xi}$$

$$r_{\xi\eta} = r_{ss} s_\xi s_\eta + r_{st} (s_\xi t_\eta + s_\eta t_\eta) + r_{tt} t_\xi t_\eta + r_s s_{\xi\eta} + r_t t_{\xi\eta}$$

$$r_{\eta\eta} = r_{ss} s_\eta^2 + 2 r_{st} s_\eta t_\eta + r_{tt} t_\eta^2 + r_s s_{\eta\eta} + r_t t_{\eta\eta}$$

$$g_{22} (s_{\xi\xi} - \phi s_\xi) - 2g_{12} s_{\xi\eta} + g_{11}(s_{\eta\eta} - \psi s_\eta) + \frac{J_2 A \cdot (\alpha r_s - \beta' r_t)}{| r_s x r_t |^2} = 0$$

$$g_{22} (t_{\xi\xi} - \phi t_\xi) - 2g_{12} t_{\xi\eta} + g_{11}(t_{\eta\eta} - \psi t_\eta) + \frac{J_2 A \cdot (\gamma r_t - \beta' r_s)}{| r_s x r_t |^2} = 0$$

where

$$J_2 = s_\xi t_\eta - s_\eta t_\xi$$

$$A = \alpha' r_{ss} - 2\beta' r_{st} + \gamma' r_{tt}$$

$$\alpha' = x_t^2 + y_t^2 + z_t^2$$

$$\beta' = x_s x_t + y_s y_t + z_s z_t$$

$$\gamma' = x_s^2 + y_s^2 + z_s^2$$

$$| r_s x r_t |^2 = (x_s y_t - y_s x_t)^2 + (x_s z_t - z_s x_t)^2 + (y_s z_t - z_s y_t)^2$$

We generate the grids on a curved surface by the following four steps:

1. Generate initial grid by algebraic method and obtain the corresponding distribution mesh in the parametric (s, t) space.
2. Compute the control functions ϕ and ψ.
3. Solve the quasi–two–dimensional elliptic system to obtain the new distribution mesh in the parametric (s, t) space.
4. The grids on the parametric (s, t) space are transformed to the physical (x, y, z) space using the Non–Uniform Rational B–Spline (NURBS) representation of the surface.

Surface Redistribution & Remapping

The NURBS representation is used for the standard surface description. The convex hull, local support, and variation diminishing properties (Ref. 14–15) of B–spline functions contribute to the generation of the well–distributed smooth grid. The parametric space associated with NURBS is transformed as the distribution (Normalized arc length based) mesh (Ref. 31, 32). The geometrical entities which are expressed into Non–NURBS form can be exactly or approximately (with desired tolerance) converted to NURBS presentation. The evaluation of derivatives $\underline{r}_s$, r_t, $\underline{r}_{ss}$, $\underline{r}_{st}$, r_{tt} . . . etc can be readily from the formulation (1). The redistributed surface grid is accomplished by evaluating the NURBS surface at the respective parameter associated with the desired distribution space. For example, the network of control points and the associated parametric space are presented in Figure 26a–b. A candidate desired distribution mesh is demonstrated in Figure 27a. The resulting redistributed surface grid is presented in Figure 27b.

It is important to note that the redistributed surface grid is obtained by evaluating the NURBS surface at the desired distribution points. Also, there exists a one–to–one correspondence between the parametric space and the control net. The straightforward search algorithm is utilized to evaluate a cell in which a desired parametric point resides. A redistributed surface resulting from a regular cubic spline surface is presented in Figure 27c. The NURBS surface is smooth and has kept the fidelity of the original surface.

Now, consider a sculptured surface presented in Figure 28a. The surface grid is mapped as a C–grid on the surface. However, if the user is interested in mapping an O–type grid on the surface then a remapping process is accomplished by essentially creating a distribution space which when evaluated results in a surface grid of Figure 28b. The associated parametric (distribution) spaces are presented in Figures 29a–b. The creation of the distribution space for remapping is intuitive and highly application dependent. The second example describing the process of remapping an O–type grid into an H–type grid is presented in Figure 30a–d. Remapping of surface grid is also required when the interior object(s) is (are) to be kept fixed as part of the interior surface grid. For example, consider the control net and the assocaited parametric space presented in Figure a–b31. An interior object on the surface is presented in Figure 32. The remapping process is needed to blend an interior object as a part of the surface grid. An interpolation – search algorithm based on the NURBS presentation is developed to evaluate parameters associated with the interior object. This evaluation is demonstrated in Figure 33. The interpolation/search algorithm utilizes derivatives $\underline{r}_s$, r_t, $\underline{r}_{ss}$, $\underline{r}_{st}$, and r_{tt} and Taylor's expansion to inversely evaluate parameters. An automatic algorithm based on the weighted transfinite interpolation (Refs. 7–9) in two dimensions is developed which blends the parameters associated with interior object into an overall distribution space. The resulting re–parameterized distribution space is demonstrated in Figure 34. The surface grid is then evaluated with respect to this new distribution space. The fidelity of the geometry associated with the interior object is kept precisely on the surface grid. The resulting remapped surface grid is presented in Figure 35.

Algebraic Surface Grid Optimization

Detailed mathematical description of this algorithm is provided in Appendix A.4. A graphical view of linear TFI v/s hermite TFI is presented in Figure 36a–d on an arbitrary configuration. The grid lines are smoother and near orthogonal in the case of Hermite TFI.

These formulations are coded in the general purpose grid system GENIE. Various computational examples have been exercised to demonstrate the success of this technique. These examples are provided in Appendix A.8 in a formal paper.

Grid Adaptation

The algorithm and a computer code for two dimensional grid adaptation is completed. This algorithm is based on the equidistribution law utilizing NURBS–algebraic technique and elliptic generation system with the forcing functions presented in previous section. This work is supported by Teledyne Brown Engineering Corporation. A technical AIAA paper containing the detailed mathematical analysis and computational examples is presented in Appendix A.3 and A.5. The definition of weighting function using the linear combination of Boolean sum of various flowfield characteristics, NURBS–algebraic regridding process maintaining the fidelity of the associated surface geometry and elliptic smoothing and rear orthogonality balance are the salient features of this algorithm.

Grid Adaptation

With structured grids, the adaptive strategy based on redistribution is by far the most simple to implement, requiring only the regeneration of the grid and interpolation of flow properties at the new grid points at each adaptive stage without modification of the flow solver unless time accuracy is desired. Time accuracy can be achieved, as far as the grid is concerned by simply transforming the time derivatives, thus adding convective–like terms that do not alter the basic conservation form of the PDEs.

Adaptive redistribution of points traces its roots to the principle of equidistributin of error [50] by which a point distribution is set so as to make the product of the spacing and a weight function constant over the points:

$$w\Delta x = constant \tag{20}$$

With the point distribution defined by a function ξ_i, where ξ varies by a unit increment between points, the equidistribution principle can be expressed as

$$w x_{\xi} = constant \tag{21}$$

This one dimensional equation can be applied in each direction in an alternating fashion [41]. A Direct extension to multiple dimensions using algebraic [32], variational, and elliptic system [33] has been developed.

Weight Function

The weight function is a very important part in the overall adaptive process. A generalized weight function applicable to various flow field characteristics has been developed. The weights are computed in all computational directions and then coupled adaptation is applied. A linear combination:

$$1 + \left(\sum_{j=1}^{N} \lambda_j w_j \right) wtf \,] \, disf, \quad \sum \lambda_j = 1 \tag{22}$$

where N = number of flow variables (e. g. pressure, temperature, density, etc.)

$$\lambda_j - \text{weighting factor associated with flow parameter } \lambda_j \geq 0 \tag{23}$$

$$\omega_j = \alpha_j\, q_j \oplus \beta_j\, k_j = \alpha_j\, q_j + \beta_j\, k_j + (\alpha_j + \beta_j - 1)\, q_j\, k_j$$

q_j – scaled gradient of the flow variable j such that $0 \le q_j \le 1$

k_j – scaled curvature values of the flow variable j such that $0 \le k_j \le 1$

wtf – weight factor that enhances the total effect of high weighted areas

disf – distribution factor that can keep the original distribution

$0 \le \alpha_j \le 1,\ 0 \le \beta_j \le 1,$

is formulated as a weight function utilizing Boolean sum of contributions from scaled gradients and curvatures. The value of the weight contribution is controlled by the weight factors and is at a maximum when gradients and/or curvature values are at a maximum. An appropriate scaling scheme [32] for weight factors α_j, β_i has been developed for proper weighting.

Algebraic Technique

The redistributed algebraic grid is generated by utilizing a surafce/volume distribution mesh as the re–parametized space associated with Non–Uniform Rational B–spline surface/volume representation. The convex hull, local support and variation diminishing properties of B–splines make NURBS an excellent choice for modeling complex geometries. The application of inverse NURBS formulation [6] allows reevaluation of control points which influences the fidelity of solid surface geometry during redistribution process.

Elliptic Technique

The elliptic generation system:

$$\sum_{i=1}^{3} \sum_{j=1}^{3} g^{ij}\, r_{\xi^i \xi^j} + \sum_{k=1}^{3} g^{kk}\, P_{k^r \xi^k} = 0$$

where r : *position vector*
g^{ij} : *contravariant metric tensor*
ξ^i : *curvilinear coordinate*
P_k : *control function* (24)

is widely utilized for grid generation [9]. The control of the characteristics and distribution of a grid system can be achieved by varying the values of the control functions P_k in Equation 24 [6]. The application of the one dimensional form of Equation 4 with Equation 20 results in the definition of control functions in three dimensions.

$$P_i = \frac{W_{\xi^i}}{W} \quad (i = 1,\ 2,\ 3) \tag{25a}$$

These control functions were generalized by Eiseman [55] as

$$P_i = \sum_{j=1}^{3} \frac{g^{ij}}{g^{ii}} \frac{(W_i)_{\xi^j}}{W_i} \quad (i = 1, 2, 3) \tag{25b}$$

In order to conserve the geometrical characteristics of the existing grid, the definition of control functions is extended as

$$P_i = (P_{initial\ geometry})_i + c_i (P_{wt}) \quad (i = 1, 2, 3) \tag{26}$$

$$(P_{initial\ geometry})^{(1)} = (P_{initial\ geometry})^{(G)}_i + c_i (P_{wt})^{(0)}$$

Grid Characteristic Analysis

A graphically interactive grid characteristic analysis software is developed. This system interactively allows surface grid to be manipulated and analyzed. The manipulation operations involve: picking line, reverse ξ and ηdirections, remove a grid line, move a point, and perform various transformations. The quality analysis include: aspect ratio, smoothing measures, orthogonality measures, area check with crossing, and measures due to interaction with solution features and grid. A pictorial view of angle checking is provided in Figure 37. A point moving operation and a line removing operation is demonstrated in Figures 38. The grid manipulation operation displays surface geometry (three–dimensional) along with its parametric space (two–dimensional) as demonstrated in Figures 39. This allows extremely easy point and line picking due to the two–dimensional parametric space. There is a one–to–one correspondence between a point on the three–dimensional surface and a point on the two–dimensional parametric space. An example of checking surface crossing is presented in Figure 40. The list of crossings found is provided in Figure 41. This list includes *(i, j)* location of possible cells.

This work is supported by a McDonnell Aircraft Company.

Domain Decomposition Strategies & Interpolation/Search Algorithms

A study to understand placement of a surface interface between blocks is performed considering flowfield simulation around a wing. This is accomplished by grid adaptive algorithm with NURBS surface re–distribution technique to evaluate the placement of blocks interfaces. The grid sizes are kept small in order to simulate flow on the workstation. Detailed description on this development is provided in Appendix A.6. A program to interpret flowfield properties at a cutting plane is developed. The program uses interpolation/search techniques to evaluate intersecting points between cutting plane and the volume and then interpolate flow properties at those points. A detailed description of this development can be found in Appendix A.7. Two additional technical papers associated with grid generation are provided in Appendix A.8 and A.9.

FLOWFIELD SIMULATIONS

Flow field simulations associated with the aforestated configurations were made. These

i. Wing/fuselage - single block configuration (Figures a-d)

ii. Vertical - horizontal tail/wing/fuselage - five block configuration (Figures 2a-b) using c-grid on the fuselage. This grid was acquired from the McDonnell Aircraft Company.

iii. Vertical - horizontal tail/wing/fuselage - five block configuration using H-O grid on the fuselage (Figures 3).

iv. Complete configuration body/inlet/nozzle (Figures 4-20).

In the wing/fuselage configurations, approximately 580,000 (173 x 42 x 80 grid for single block) grid points were used. Approximately 2.2 million grid points were used in the C-H tail/wing/fuselage configuration.

A technique to re-distribute surface grids using Non-Uniform Rational B-spline (NURBS) representation has been developed. The NURBS representation allows the redistribution of grid points on the surface while maintaining fidelity of the surface geometry (Ref. 31). Flowfield simulations using similar physical conditions and grids were also performed on the Connection Machine (CM-200) in parallel. A redistributed surface grid for the vertical-horizontal tail/wing/fuselage, configuration *iii*, is presented in Figure 3.

A comparative study is made between two popular algorithms.

The first algorithm is based on Roe's approximate Riemann solver as implemented by Whitfield (Ref. 20). This scheme solves the time-dependent Reynolds-averaged Navier-Stokes equations in generalized time-dependent curvilinear coordinate systems. Accuracy is achieved by a conservative finite-volume discretization which satisfies the geometric conservation law generalized to moving coordinate systems. The flow solver code is written in a block-structured form allowing calculations with nearly unrestricted arrangement of arbitrarily sized blocks (Ref. 21). Upwind differencing is used for the inviscid terms and centered differencing is used for the viscous and diffusive terms. The inviscid flux vectors in the residual are computed using the flux difference split theory. To summarize the approach, Roe averaging (Ref. 22) was used to determine the numerical flux at cell faces with the schemes of Osher and Chakravarthy (Ref. 23) applied to achieve second or third-order spatial accuracy . There is some deviation in construction of the higher-order schemes from that put forth in (Ref. 23) as discussed in (Ref. 20). In keeping with the upwind nature of evaluating the inviscid flux vectors in the residual, the implicit operator is also upwinded. However, it was found in (Ref. 20) that convergence was much improved if flux vector splitting (Ref. 24) was used in the implicit operator of the equation rather than flux difference splitting. The viscous and diffusive terms are treated explicitly, and the turbulence effects are modeled with the well-known Baldwin and Lomax mixing length model (Ref. 25), although present compilations were made using an inviscid model. A mathematical description of this algorithm is provided in Appendix A11.

The second code applied is the PARC3D code as developed by Cooper and Sirbaugh (Ref. 26) at the Arnold Engineering Development Center (AEDC). This code also solves either the Navier-Stokes equations or the Euler equations, subject to user specification. PARC3D is a finite-difference code which applies standard central difference discretization of the system of PDE's. Jameson style artificial dissipation is applied to maintain stability. The resulting system of equations was solved herein by application of Pulliam's (Ref. 27) diagonalized Beam and Warming approximate factor-

ization algorithm. Among other characteristics, PARC3D utilizes conservative metric differencing, offers local time–step options, and provides a generalized boundary condition treatment. The code can be applied in either a single or multi–block mode. This results in a code which is quite general and easy to apply to complex configurations.

Since the architecture of the Single Instruction Multiple Data Stream Machine (SIMD) is well suited for an explicit type method, an explicit multi–stage multi–block full Navier–Stokes solver developed by Patel, Sturek, and Smith (Ref. 28) is utilized for parallel computations. This code allows multi–zone overlaid grids. To maintain stability adaptive artificial dissipation terms based on a directional eigenvalue scaling (Ref. 29) have been added to the equations. A local time stepping scheme which is well suited for parallel processing is developed.

Preliminary computations have been performed simulating the flow field about the F15e wing/fuselage configuration at a Mach number of 1.5 and an angle of attack of 0.0. The simulation for the grids *ii* and *iii* including the vertical and horizontal tail is underway.

The simulations were made by application of the previously mentioned Roe finite volume scheme (EAGLE) and the Beam–Warming finite difference scheme (PARC3D). The PARC3D simulation was made as a single block computation whereas the EAGLE simulation was made on the same grid split into two contiguous blocks. This was done to satisfy in–core memory requirements for the UBIFLOW code.

Macroscopic flow features for the two computations agree quite well as evidenced by comparing Mach number contours on the fuselage and wing surfaces (Figures 42 and 43). The magnitude of the Mach number as well as the compression and expansion patterns match reasonably well. Close examination of the respective contours reveals the Roe scheme as an apparently less dissipative solution which is consistent with anticipated results. Representative quantitative comparison of computed wing pressure distributions are shown on the upper surface at 50% chord and on the lower surface at 25% chord in Figures 44 and 45. These, and other supporting figures, illustrate similar overall levels of agreement. However, disagreement is observed, most notably on the lower surface near the wing tip. Also general disagreement is noted near the leading and trailing edge.

The computations at a Mach number of 0.98 and an angle of attack of 1.1 degrees will be compared with experiment. These simulations are being made on a more realistic grid *(ii* and *iii)* representing the fuselage/wing/vertical and horizontal tail assembly. Integrated parameters, such as lift coefficient, will also be compared to assess the overall significance of discrepancies within the solutions. These computations are partially complete and a request for access to experimental data has been made.

An additional demonstration of capability is made by presenting results of a simulation of the fuselage/wing/vertical and horizontal tail assembly by application of an explicit CFD code executing on a parallel computer architecture. The computation was made to simulate conditions at Mach 1.5 and 0.0 angle of attack. Representative results are shown in the form of surface pressure distribution (Figure 46). These results will be compared with computations made with the implicit Roe scheme.

One results of this research was the development of various advanced techniques needed to efficiently solve problems encountered during the F15 grid generation process.

REFERENCES

1. Kutler, P., "A Perspective of Theoretical and Applied Computational Fluid Dynamics", AIAA–83–0037, 1983.

2. Phares, W. J., Cooper, G. K., Swafford, T. W., Jones, R. R., "Application of Computational Fluid Dynamics to Test Facility and Experimental Design", AIAA–86–1733, June 1986.

3. Droegemeier, K. K., "Numerical Simulation of Thunderstorm Outflows and Microbursts", *CRAY CHANNELS*, p. 18, Summer 1987.

4. Thompson, J. F., "Composite Grid Generation for General Three–Dimensional Regions – The EAGLE Code", *AIAA Journal*, Vol. 26, No. 3, p. 271, March 1988.

5. Thompson, J. F., "A Composite Grid Generation for General Three–Dimensional Regions – The EAGLE Code", *AIAA Journal*, Vol. 26, No. 3, p. 271, March 1988.

6. Thompson, J. F., "Program EAGLE–numerical grid Generation System User's Manual", Vols. II, III, AFATL–TR–87–15, March 1987.

7. Soni, B. K., "GENIE: GENeration of Computational Geometry–Grids for Internal–External Flow Configurations", *Proceedings of the Numerical Grid Generation in Computational Fluid Dynamics '88*, Miami, FL, 1988.

8. Soni, B. K., McClure, M. D. and Mastin, C. W., "Geometry and Generation in N+1 Easy Steps", *The First International Conference on Numerical Grid Generation in Computational Fluid Dynamics '88*, Miami, FL, 1988.

9. Soni, B. K., "Two and Three–Dimensional Grid Generation for Internal Flow Applications of Computational Fluid Dynamics", AIAA–85–1526.

10. Cooper, G. K., "The PARC Code: Theory and Usage", AEDC–TR–87–24, Arnold AFB, TN, October 1987.

11. Whitfield, D. L., "Implicit Upwind Finite Volume Scheme for the Three–Dimensional Euler Equations", *Engineering and Industrial Research Station Report*, Mississippi State University, MSSU–EIRS–ASE–85–1, September 1985.

12. Whitfield, D. L., Janus, J. M. and Simpson, L. B., "Implicit Finite Volume High Resolution Wave–Split Scheme for Solving the Unsteady Three–Dimensional Euler and Navier–Stokes Equations on Stationary or Dynamic Grids", *Engineering and Industrial Research Station Report*, Mississippi State University, No. MSSU–EIRS–ASE–88–2, August 1987.

13. Soni, B. K., Yu, T.–Y., and Vaughn, D., "CAGI: Computer Aided Grid Interface: A CFD Pre–Processor", *Proceedings of the CFD Workshop for Rocket Propulsion Applications*, NASA Marshall Space Flight Center, Huntsville, AL, April 1992.

14. Farin, G., "Curves and Surfaces for Computer Aided Geometric Design: A Practical Guide", Academic Press, 1990.

15. deBoor, C., "A Practical Guide to Splines", Springer, 1978.

16. Steinbrenner, J. and Foiits, C., "GRIDGEN: User's Manual", Wright Research and Development Center and General Dynamics, Fort Worth Division, 1990.

17. Sorenson, R. L., "Three–Dimensional Zonal Grids About Arbitrary Shapes by Poisson's Equation", *Numerical Grid Generation for Computational Fluid Mechanics '88*, p. 88, Pineridge Press.

18. Steger, J. L. and Chaussee, D. S., "Generation of Body–Fitted Coordinates Using Hyperbolic Partial Differential Equations", *SIAM Journal of Scientific Statistic Computation*, p. 431, 1980.

19. Soni, B. K., Thompson, J. F., Stokes, M. and Shih, M.–H., "GENIE $^{++}$, EAGLEView and TIGER: A General Purpose as Special Purpose Graphically Interactive Grid Systems", AIAA–92–0071.

20. Whitfield, D. L., Janus, J. M. and Simpson, L. B., "Implicit Finite Volume High Resolution Wave–Split Scheme for Solving the Unsteady Three–Dimensional Euler and Navier–Stokes Equations on Stationary or Dynamic Grids", *Engineering and Industrial Research Station Report*, Mississippi State University, No. MSSU–EIRS–ASE–88–2, February 1988.

21. Arabshahi, A. and Whitfield, D. L., "A Multiblock Approach to Solving the Three–Dimensional Unsteady Euler Equations about A Wing–Pylon–Store Configuration:, AIAA–89–3401–CP, August 1989.

22. Roe, P. L., "Approximate Riemann Solvers, Parameter Vector, and Difference Schemes", *Journal of Computational Physics,* Vol. 43, p. 357, 1981.

23. Osher, S. and Charavarthy, S., "Very High Order Accurate TVD Schemes", *ICASE Report No. 84–44*, September 1984.

24. Steger, J. L. and Warming, R. F., "Flux Vector Splitting of the Inviscid Gasdynamic Equations with Applications to Finite Difference Methods", *Journal of Computational Physics*, Vol. 40, p. 263, 1981.

25. Baldwin, B. S. and Lomax, H., "Thin–Layer Approximation and Algebraic Model for Separated Turbulent Flows", AIAA–78–257, January 1978.

26. Cooper, G. R. and Sirbaugh, J. R., "The PARC Distinction: A Practical Flow Simulator", AIAA–90–2002, *AIAA/ASME/SAE/ASEE 26th Joint Propulsion Conference,* Orlando, FL, July 1990.

27. Pulliam, J. H., "Euler and Thin Layer Navier–Stokes Codes: ARC2D, ARC3D", *Notes for Computational Fluid Dynamics User's Workshop*, The University of Tennessee Space Institute, Tullahoma, TN, UTSI Publication E02–4005–023–84, p. 15.1, March 12–16, 1984,.

28. Patel, N. R., Sturek, W. B. and Smith, G. A., "Parallel Computation of Supersonic Flows Using a Three–Dimensional, Zonal, Navier–Stokes Code", BRL–TR–30XX, November 1988.

29. Swanson, R. C. and Turkel, E., "Artificial Dissipation and Central Difference Schemes for The Euler and Navier–Stokes Equations", *AIAA 8th Computational Fluid Dynamics Conference,* Honolulu, HA, June 1987.

30. Soni, B. K., Weatherill, N. P., Thompson, J. F., "Grid Adaptive Strategies in CFD", *International Conference on HydroScience & Engineering,* Washington, DC, June 1993.

31. Soni, B. K., Huddleston, D. H., Arabshahi, A., Vu, B., Patel, N., Clarke, and Coleman, M., "A Study of CFD Algorithms Applied to Complete Aircraft Configurations", AIAA–93–0784, *AIAA 31st Aerospace Sciences Meeting,* Reno, NV, January 1993.

32. Yang, J. C., Soni, B. K., "Structured Adaptive–Grid Generation", accepted for publication, *Journal of Applied Mathematics & Computations,* 1993.

33. Thompson, J. F. and Gatlin, B., "Easy EAGLE: An Introduction to the EAGLE Grid Code", Mississippi State University, 1988.

34. Thompson, J. F., "A General Three–Dimensional Elliptic Grid Generation System on A Composite Block Structure", *Computer Methods in Applied Mechanics & Engineering*, p. 377, 1987.

35. Remotigue, M. G., Hart, E. T. and Stokes, M. L., "EAGLEView: A Surface and Grid Generation Program and Its Data Management", NASA, CP–3143, p. 319, *Proceedings of a Workshop*, NASA Langley Research Center, Hampton, VA, April 1992.

36. Soni, B., "Grid Generation for Internal Flow Configurations", *Journal of Computers & Mathematics with Applications,* Vol. 25, No. 5/6, September 1992.

37. Steinbrenner, J. P. and Chauner, J. R., "Recent Enhancements to the GRIDGEN Structured Grid Generation System", NASA, CP–3143, p. 253, *Proceedings of a Workshop,* NASA Langley Research Center, Hampton, VA, April 1992.

38. Sorenson, R. L., "GRAPEVINE: Grids About Anything by Poisson's Equations in A Visually Interactive Networking Environment, NASA, CP–3143, p. 319, *Proceedings of a Workshop,* NASA Langley Research Center, Hampton, VA, April 1992.

39. Akdag, V. and Wulf, A., "Integrated Geometry and Grid Generation System for Complex Configurations", NASA CP–3143, p. 161, *Proceedings of a Workshop,* Hampton, VA, April 1992.

40. Dener, C. and Hirsch, C., "IGG – An Advanced Interactive Grid Generation System", p. 503, *Proceedings of the Third International Conference on Numerical Grid Generation in Computational Fluid Dynamics and Related Fields.* Barcelona, Spain, June 1991.

41. Soni, B. K. and Yang, J. L., "General Purpose Adaptive Grid System", AIAA–92–0664, *AIAA 30th Aerospace Sciences Meeting,* Reno, NV, January 1992.

42. Jameson, A., Schmidt, N. and Turkel, E., "Numerical Solutions of the Euler Equations by Finite Volume Methods Using Runge–Kutta Time–Stepping Schemer", AIAA–81–1259, *AIAA 14th Fluid and Plasma Dynamics Conference,* Palo Alto, CA, 1981.

43. Patel, N. R., Sturek, W. B. and Smith, G. A., "Parallel Computation of Supersonic Flows Using a Three–Dimensional, Zonal, Navier–Stokes Code", BRL–TR–30XX, November 1988.

44. Swanson, R. C. and Turkel, E., "Artificial Dissipation and Central Differnece Schemes for the Euler and Navier–Stokes Equations", *AIAA 8th Computational Fluid Dynamics Conference,* Honolulu, HA, June 1987.

45. Soni, B. K., Weatherill, N. P., Thompson, J. F., "Structured–Unstructured and Adaptive Grid Techniques in the National Grid Project", *The Second U. S. Congress on Computational Mechanics,* June 1993.

46. Yu, T.–Y., "IGES Transformer and NURBS in Grid Generation", Master Thesis in Aerosapce Engineering, Mississippi State University, Mississippi State University, Mississippi, MS 1992.

47. Yoon, Y.–H., "Enhancements and Extensions of EAGLE Grid Generation System", Ph. D. Dissertation, Mississippi State University, Mississippi State, MS, 1991.

48. Thompson, J. F., Warsi, Z. U. A., and Mastin, C., W., "Numerical Grid Generation: Foundations and Applications", North Holland Publisher.

49. Soni, B. K., "Grid Optimization: A Mixed Approach", *Proceedings of the 3rd International Conference of Numerical Grid Generation in Computational Fluid Dynamics,* Barcelona, Spain, June 1991, edited by A. S. Arcilla, J. Hauser, P. R. Eiseman and J. F. Thompson: North Holland.

50. Thompson, J. F., "A Survey of Dynamically–Adaptive Grids in the Numerical Solution of Partial Differential Equations", *Applied Numerical Mathematics 1,* p. 3, North–Holland, 1985.

51. Connett, W. C., Agarwal, R. K., and Schwartz, A. L., "An Adaptive Grid–Generation Scheme for Flow Field Calculations", AIAA–87–0199.

52. Abolhassani, J. S., Smith, R. E. and Surendra, N. T., "Grid Adaptation for Hypersonic Flow", AIAA–87–1169.

53. Yamaguchi, F., "Curves and Surfaces in Computer Aided Geometric Design", Springer–Verlag, 1988.

54. Dwyer, H. A., "Grid Adaptation for Problem in Fluid Dynamics", *AIAA Journal,* Vol. 22, No. 12, December 1984.

55. Eiseman, P. R., "Alternating Direction Adaptive Grid Generation", AIAA–83–1937, 1983.

56. Jameson, A., Baker, T. J. and Weatherill, N. P., "Calculation of Inviscid Transonic Flow Over A Complete Aircraft", AIAA–86–0103, 1986.

57. Marchant, M. J. and Weatherill, N. P., "The Construction of Nearly Orthogonal Multiblock Grids for Compressible Flow Simulation", *Communications in Applied Numerical Methods,* 1993.

58. Nakashashi, K. and Deiwert, G. S., "Three–Dimensional Adaptive Grid Method", *AIAA Journal,* Vol. 24, p. 948, 1986.

59. Thompson, J. F. and Mastin, C. W., "Order of Difference Expressions in Curvilinear Coordinate Systems", *Journal of Fluids Engineering,* Vol. 107, P. 241, 1985.

60. Weatherill, N. P. and Soni, B., "Grid Generation – Refinement in Structured–Unstructured Algorithms", *Proceedings of the 3rd International Conference of Numerical Grid Generation in Computational Fluid Dynamics,* Barcelona, Spain, June, edited by A. S. Arcilla, J. Hauser, P. R. Eiseman and J. F. Thompson, North Holland, p. 143, 1991.

61. Weatherill, N. P., "Mixed Structured–Unstructured Meshes for Aerodynamic Flow Simulation", *The Aeronautical Journal,* Vol. 94, p. 111–123, No. 934, 1990.

62. Weatherill, N. P., Hassan, O. and Marcum, D. L., "Adaptive Inviscid Flow Solutions for Aerospace Geometries on Efficiently Genreated Unstructured Tetrahedral Meshes", AIAA–93–0341, *AIAA Aerospace Sciences Conference,* January 1993.

63. Kutler, P., "A Perspective of Theoretical and Applied Computational Fluid Dynamics", AIAA–83–0037, 1983.

64. Phares, W. J., Cooper, G. K., Swafford, T. W., Jones, R. R., "Application of Computational Fluid Dynamics to Test Facility and Experimental Design", AIAA–86–1733, June 1986.

65. Droegemeier, K. K., "Numerical Simulation of Thunderstorm Outflows and Microbursts", *CRAY CHANNELS,* p. 18, Summer 1987.

66. Kent, R., IGES Editor, *IGES/PDES Organization Spline Curves & Surfaces in the Initial Graphics Exchange Specification (IGES)* version 5.0 Appendix B, p. 417–422.

67. Soni, B. K., "Elliptic Grid Generation System: Control Functions Revisited", *Journal of Applied Mathematics & Computers.*

68. Soni, B. K., "An Efficient and Robust Algorithm for Grid Refinement", to be published.

69. Cooper, G. K., Sirbaugh, J. R., "PARC Code: Theory and Usage", AEDC–TR–89–15, *Arnold Engineering Development Center,* Arnold AFB.

70. Yang, J. C., "General Purpose Adaptive Grid Generation System", Ph. D. Dissertation, Mississippi State University, Mississippi State, MS, July 1993.

71. Brackbill, J. U. and Saltzman, J. S., "Adaptive Zoning for Singular Problems in Two Dimension", *Journal of Computational Physics,* Vol. 46, p. 342, 1982.

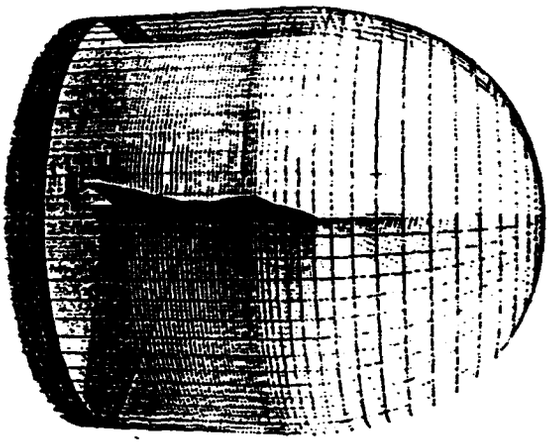

Figure 1a. Wing/fuselage overall configuration

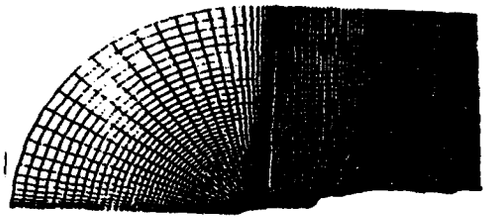

Figure 1b. J = constant grid surface

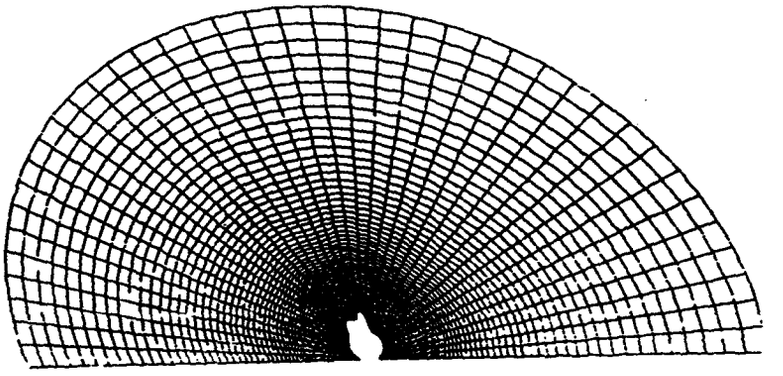

Figure 1c. I = constant surface (I = 173)

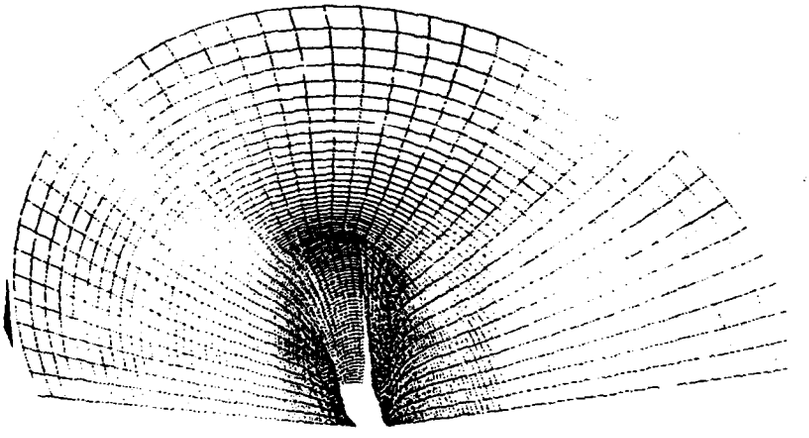

Figure 1d. Grid behavior at I = constant cutting through wing

Figure 1. F15 Wing/Fuselage Grid (173 x 42 x 80)

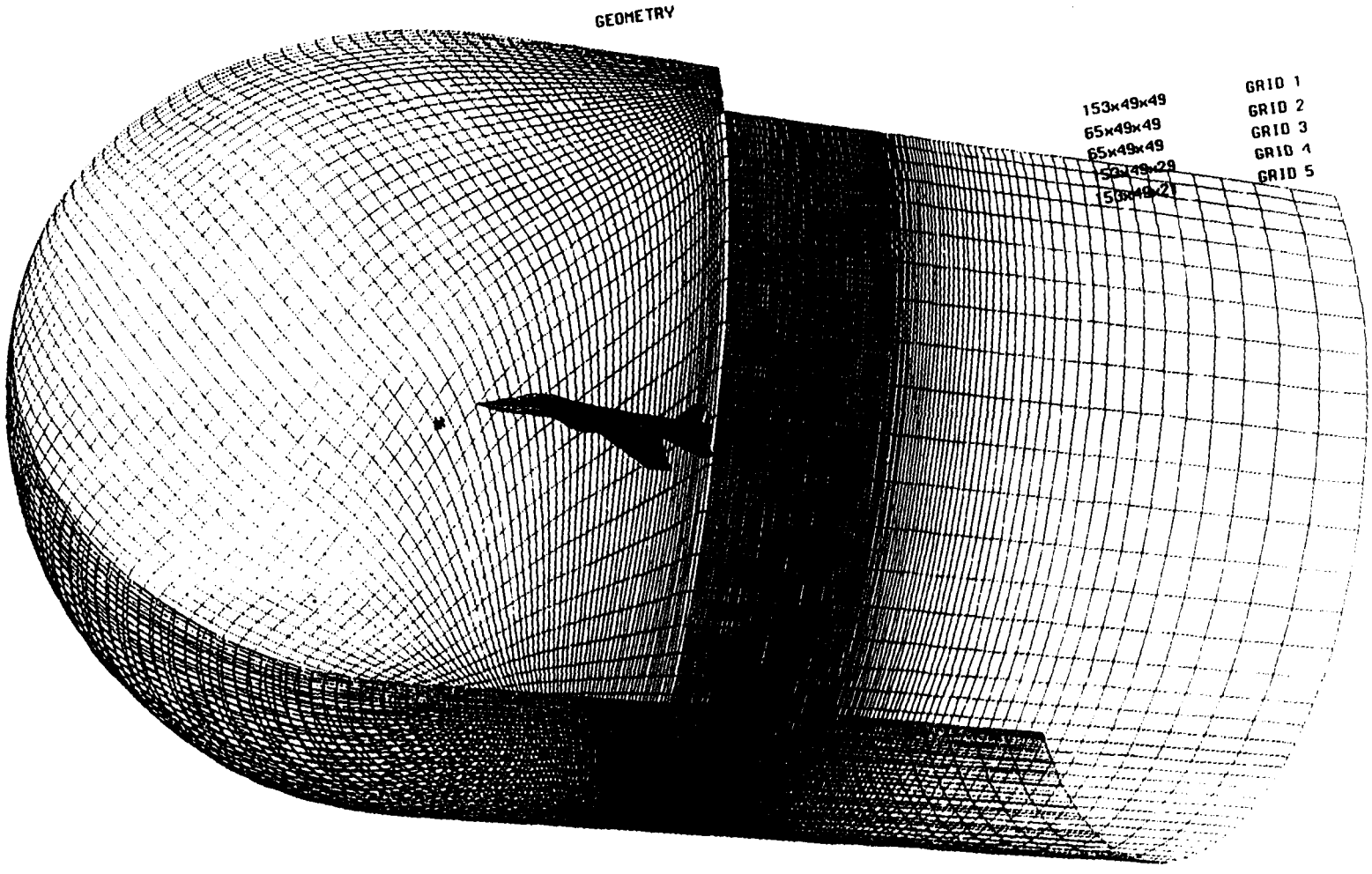

Figure 2a. F15e Vertical-Horizontal Fin/Wing/Fuselage Five Block Configuration

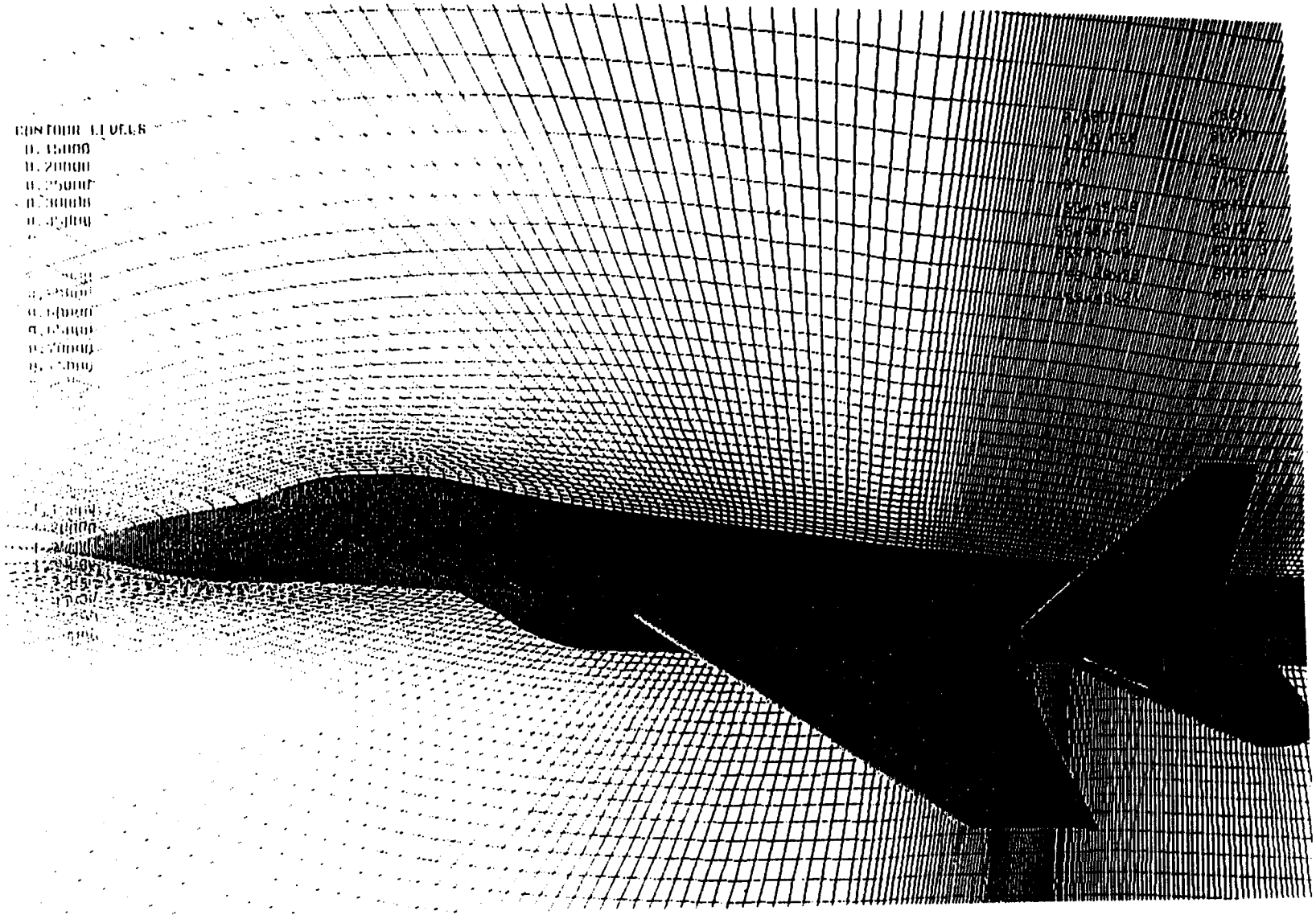

Figure 2b. Cross Sectional View of Grid and Configuration

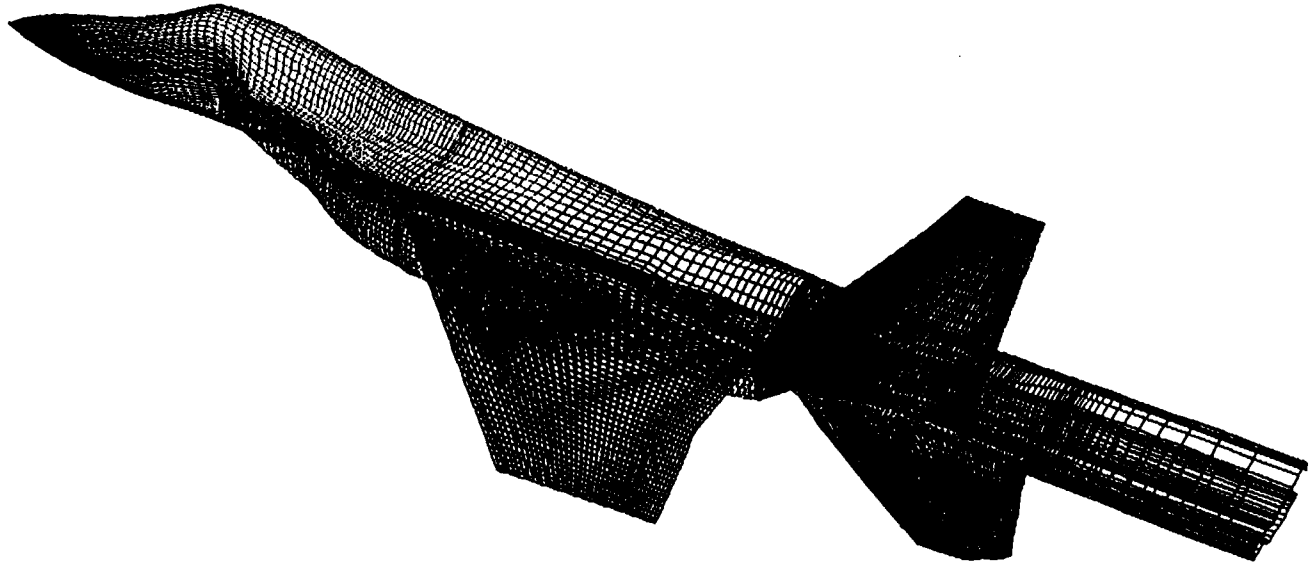

Figure 3. Vertical-Horizontal/Wing/Fuselage Configurations

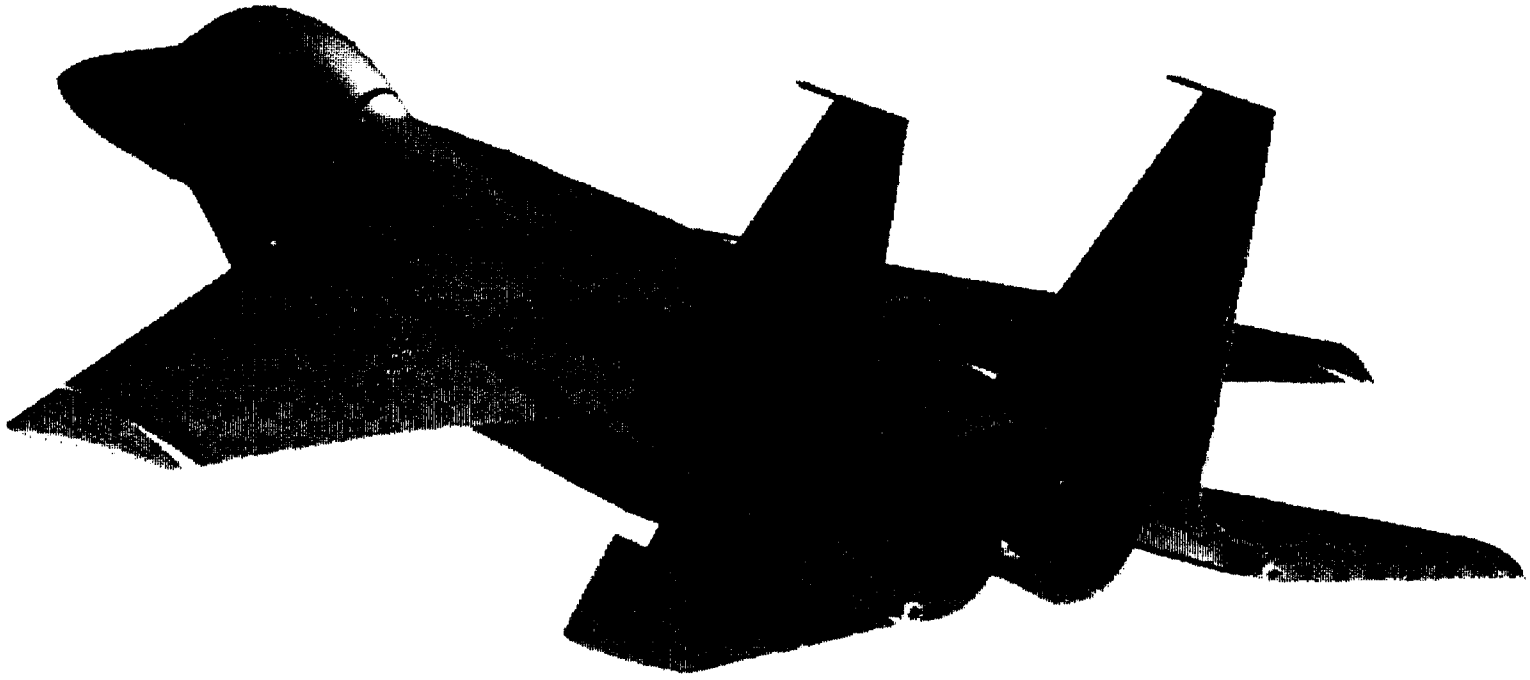

F-15
ORIGINAL GEOMETRY DATA

Figure 4. F15 Full Geometry As Defined By the 49 Sculptured Surfaces

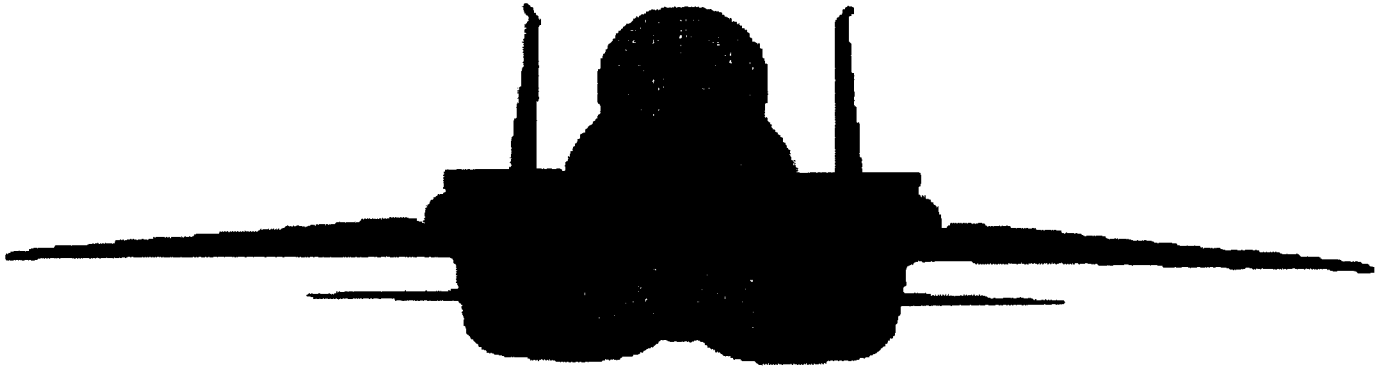

F-15

HEAD-ON VIEW
OF ORIGINAL GEOMETRY

Figure 5. Frontal Profile of Original CAD Geometry

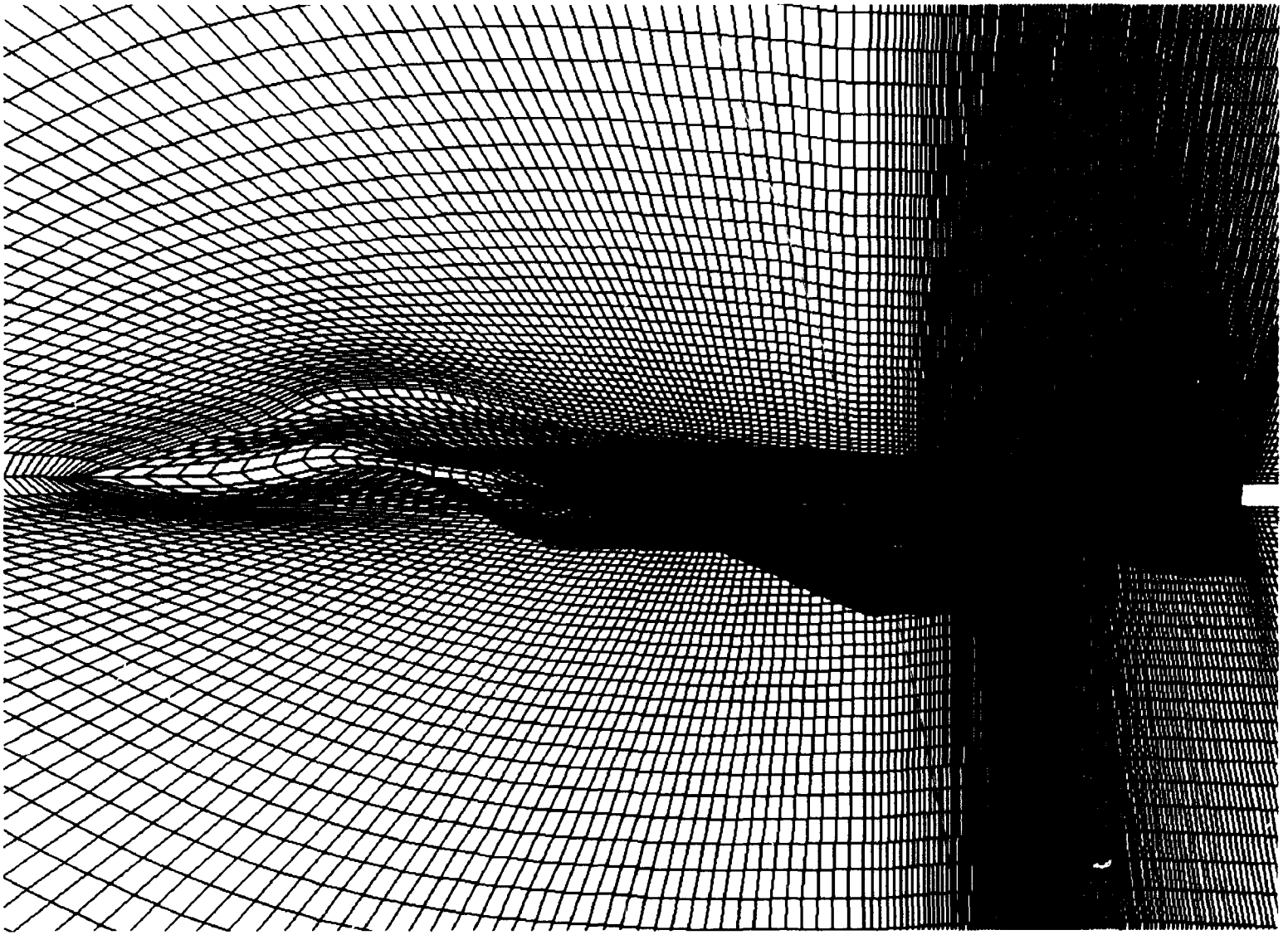

Figure 6. 5-Block Wing/Body/Tail Configuration With Grid Planes

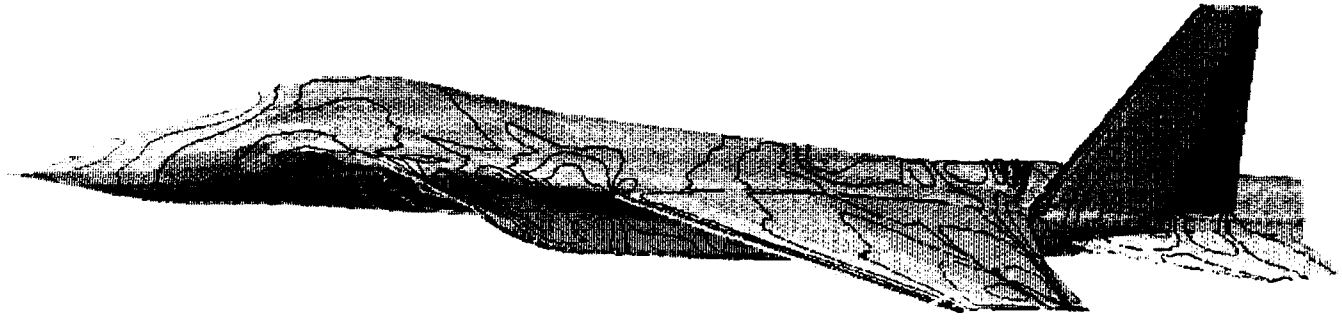

F–15

PRESSURE CONTOURS ON SURFACE

Figure 7. Wing/Body/Tail Configuration Solution As Obtained By Ubiflow

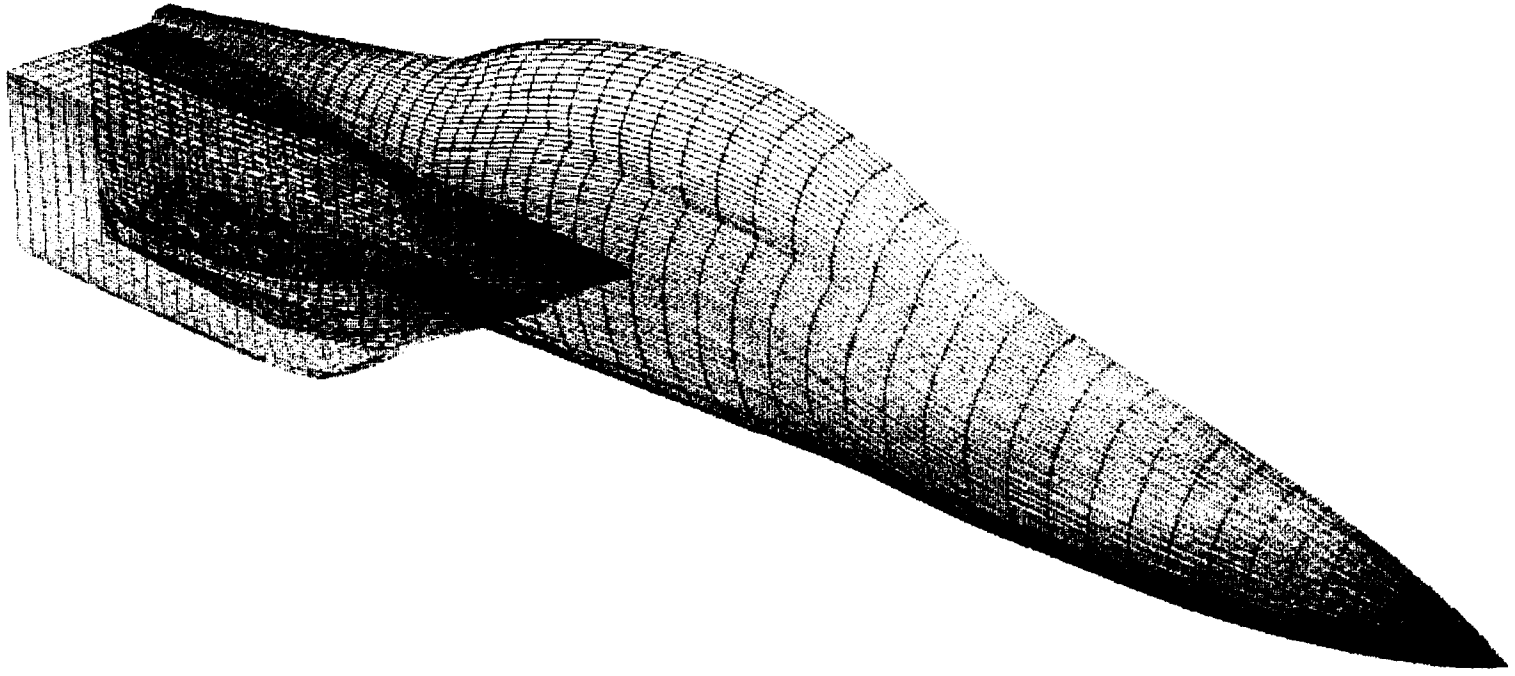

F–15

INLET GEOMETRY FROM ORIGINAL DATA

Figure 8. Inlet Geometry of Special Interest In Surface Grid Modeling

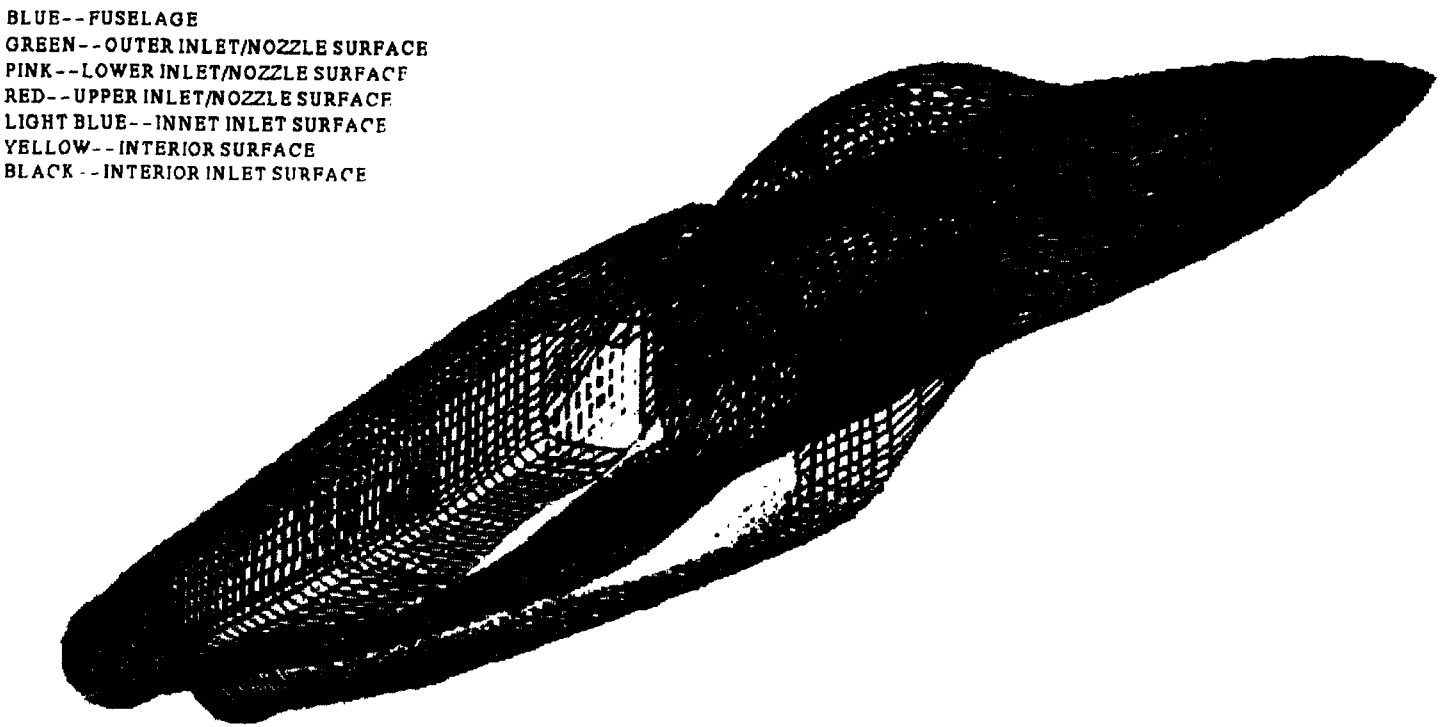

F–15

FRONTAL VIEW OF SURFACE GRID

Figure 9. Full Surface Grid of Body/Inlet/Nozzle Configuration Created With Genie++

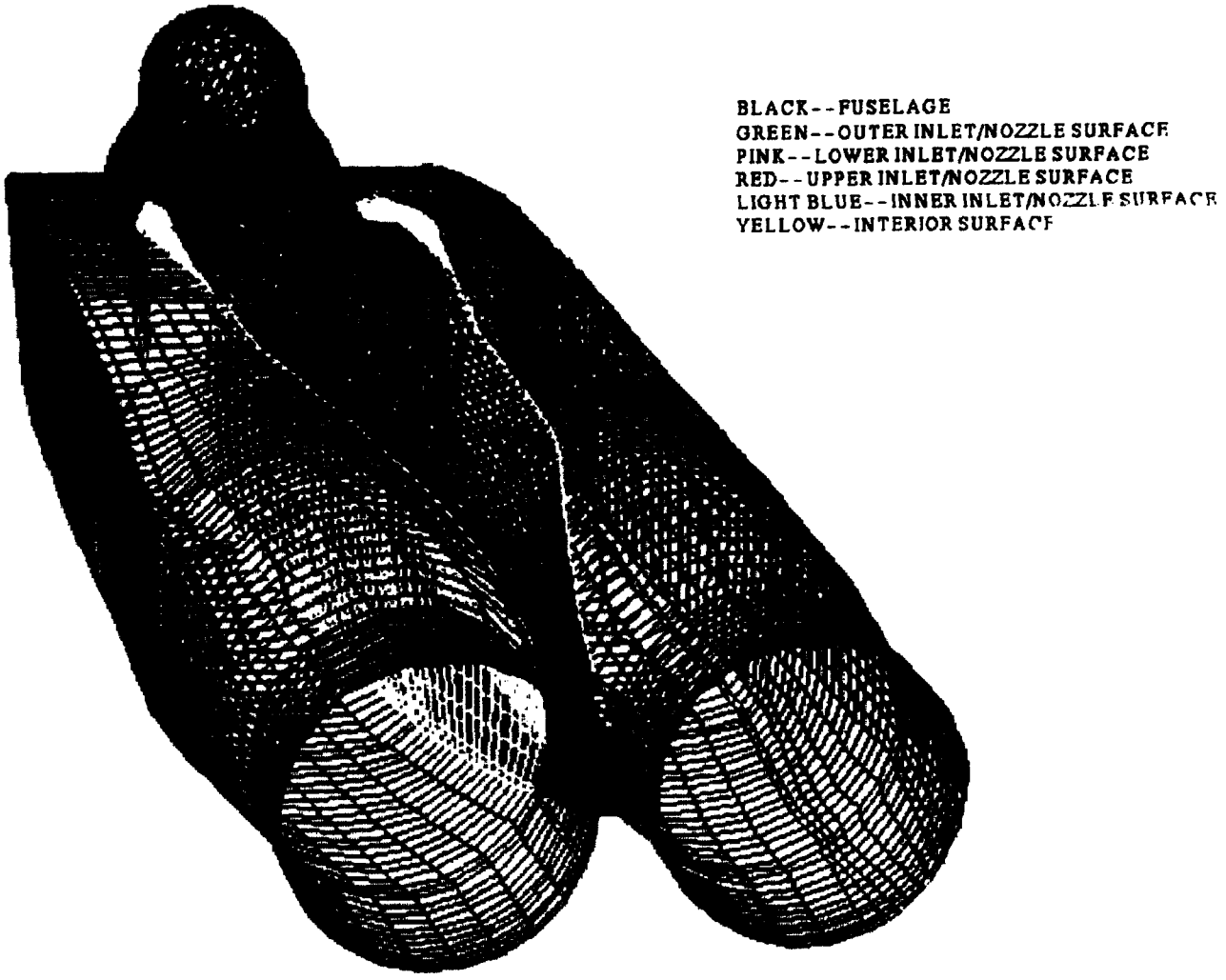

F-15

REAR VIEW OF SURFACE GRID

Figure 10. Rear Perspective of Genie Surface Grid Showing Nozzle Geometry

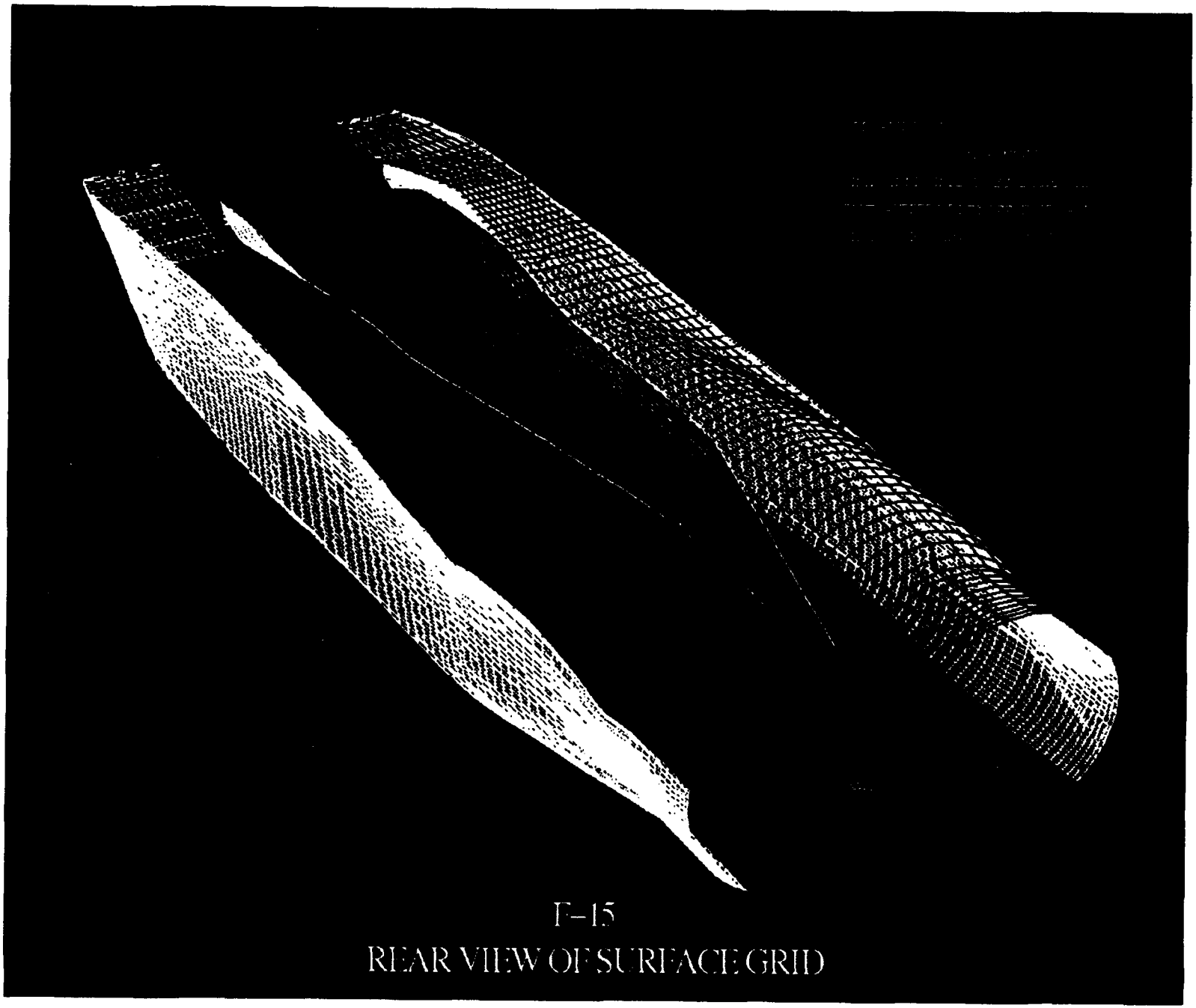

Figure 11. Full Surface Grid As Seen From Rear

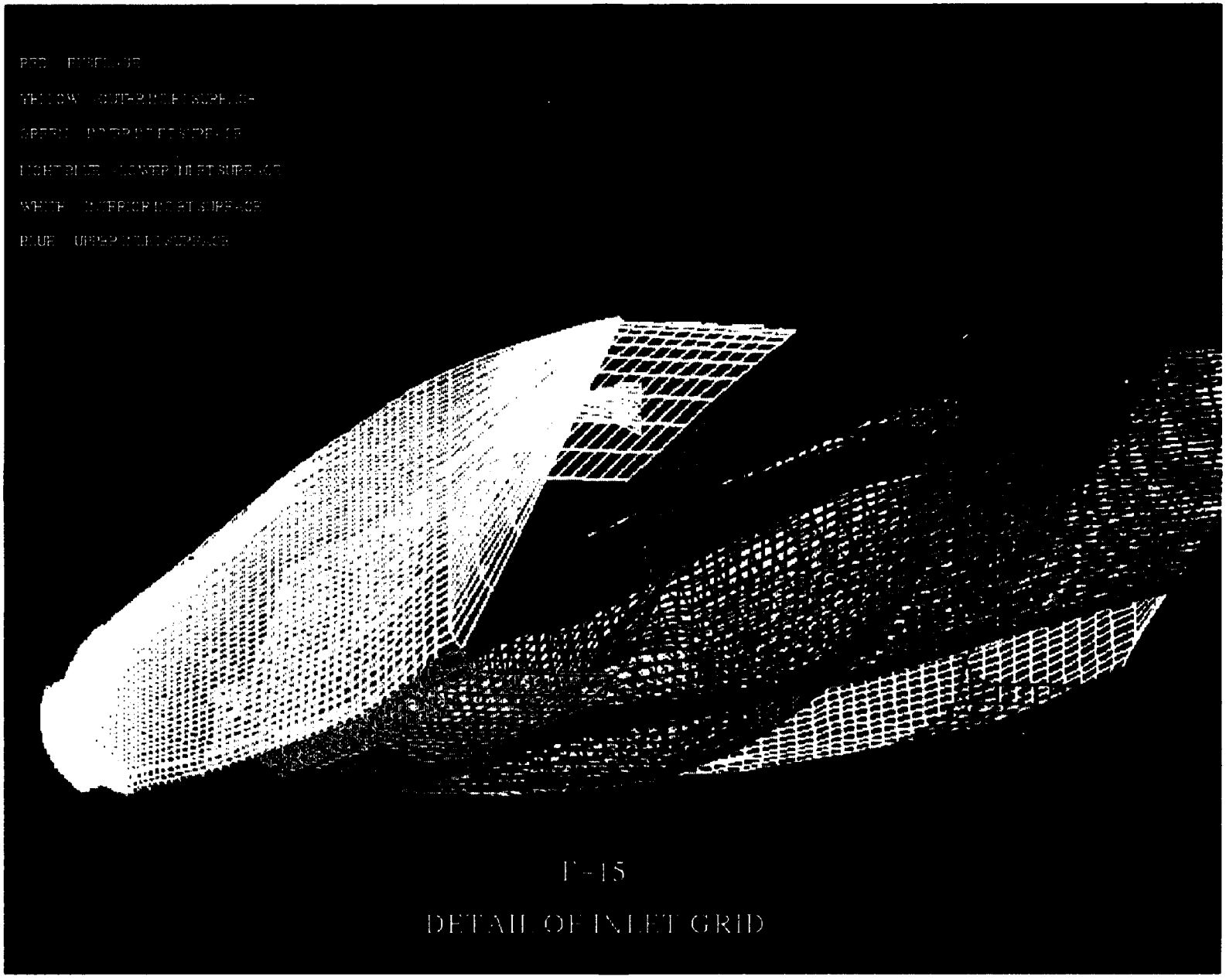

Figure 12. Detailed Look At The Inlet Geometry Modeled Using Genie++

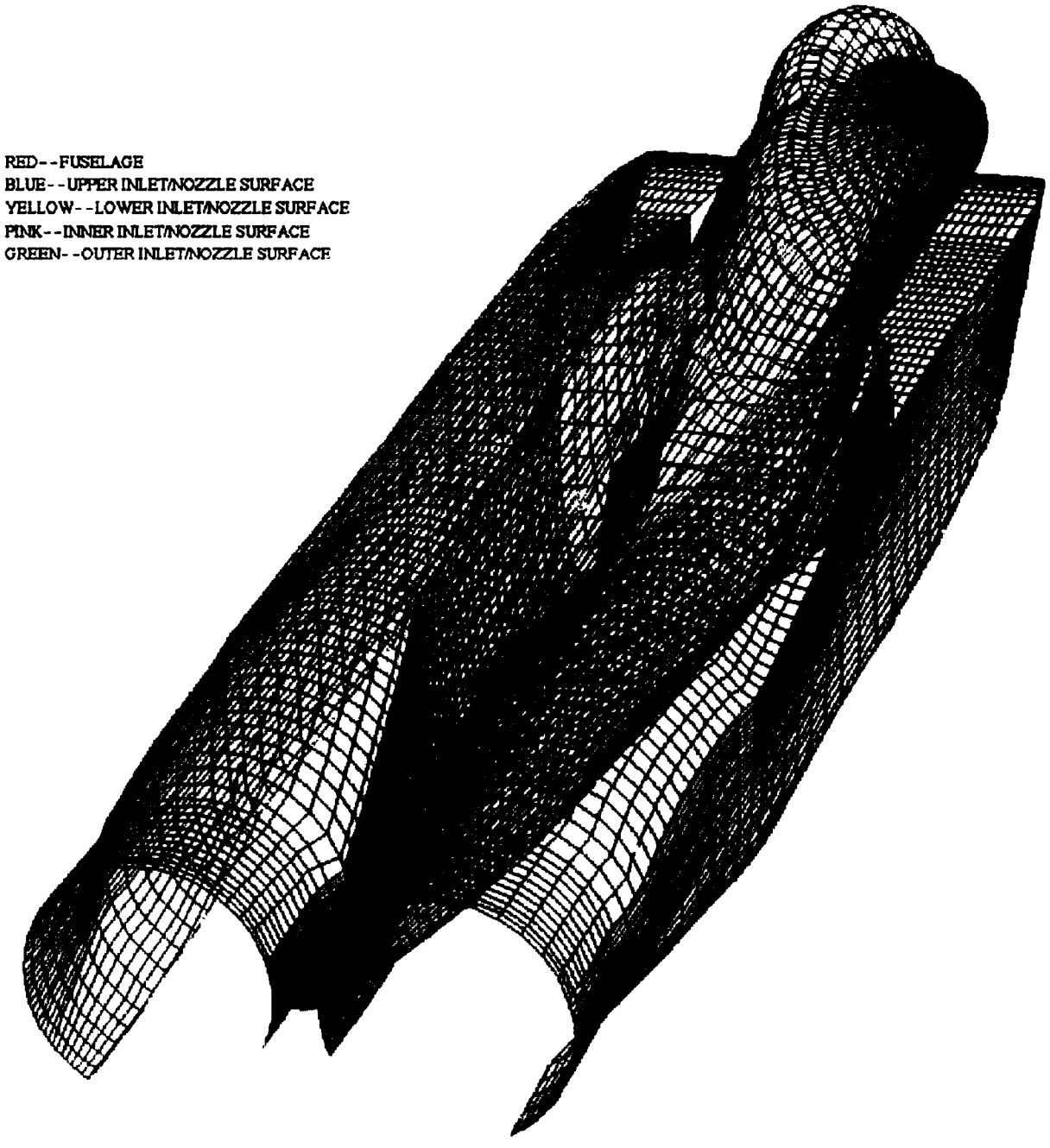

F-15

DETAIL OF NOZZLE GRID

Figure 13. View of Nozzle Surfaces

Figure 14. Body/Inlet/Nozzle Configuration Genie Surface Grid

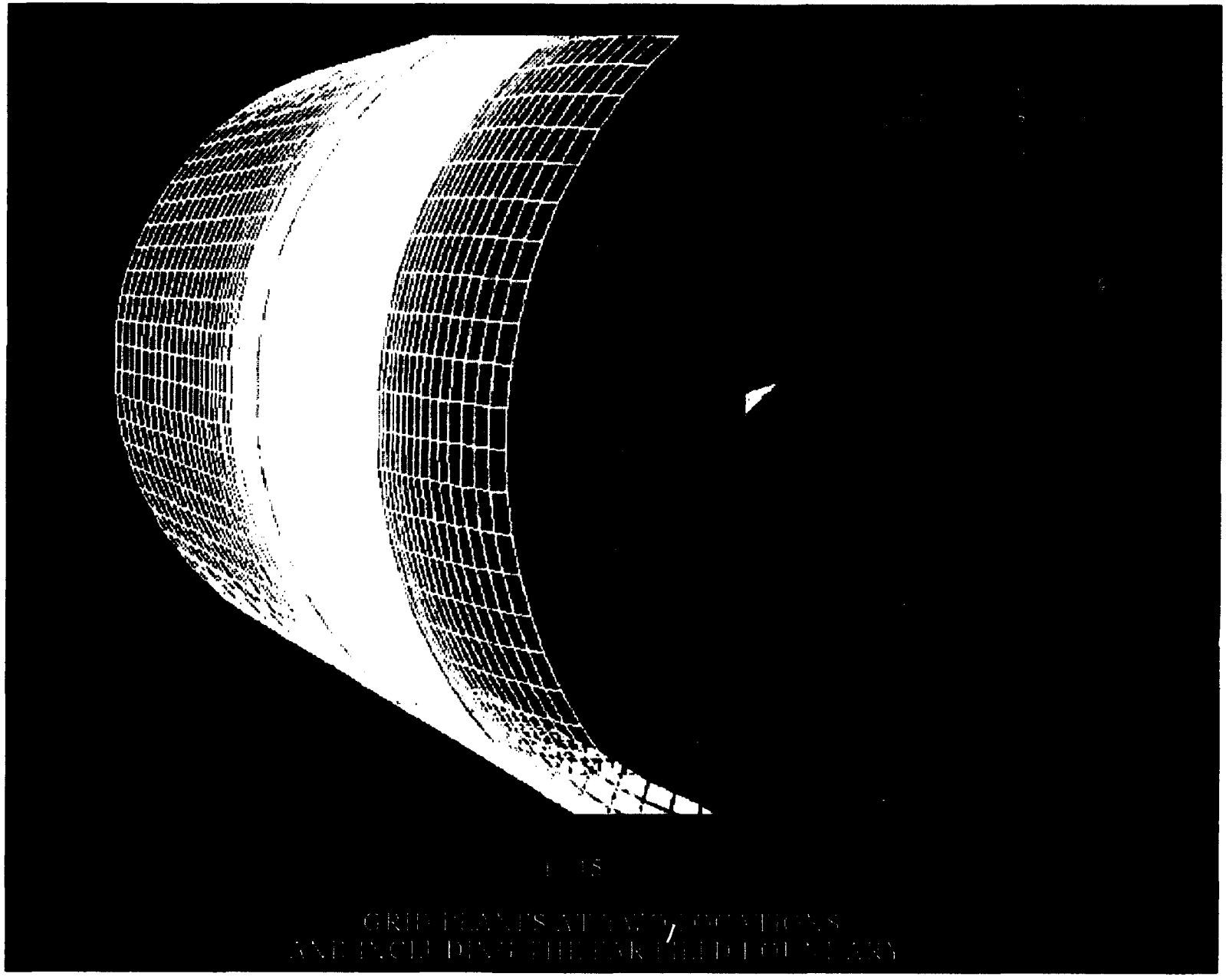

Figure 15. View of Overall Volume Grid Showing General Point Distribution and Outer Boundary

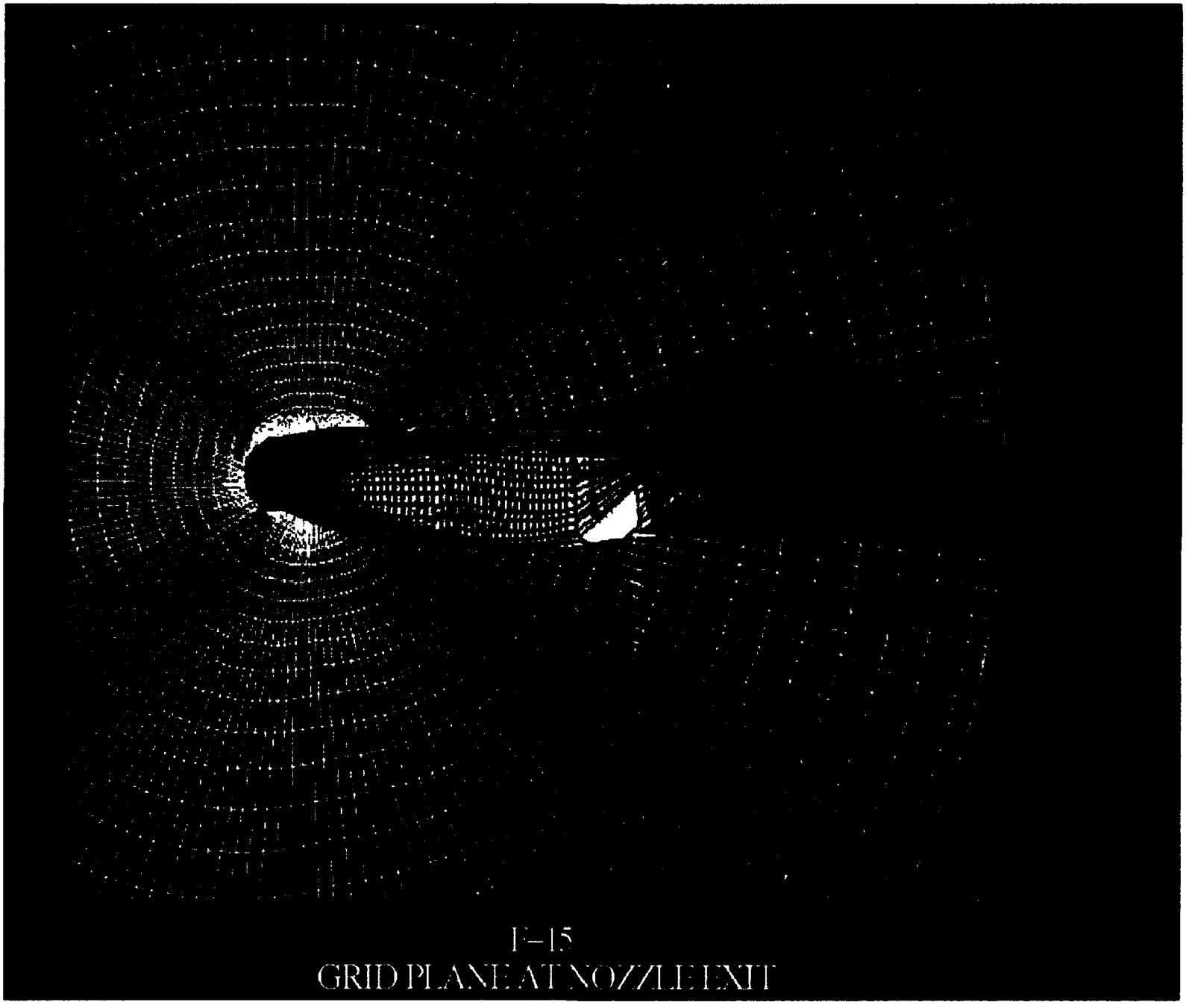

Figure 16. J-Constant Grid Surface At Nozzle

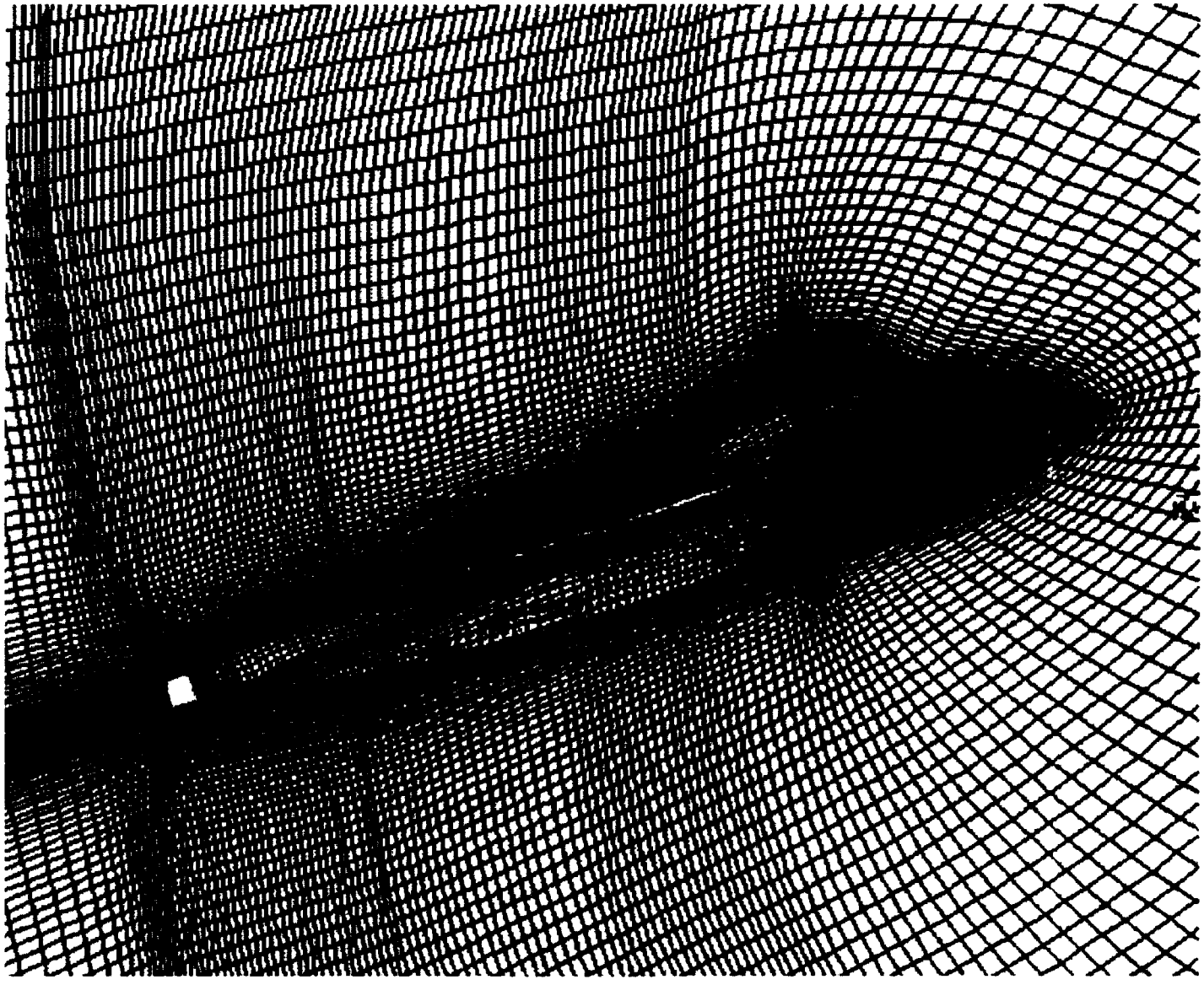

Figure 17. I-Constant Grid Surfaces Showing Point Clustering Near Body

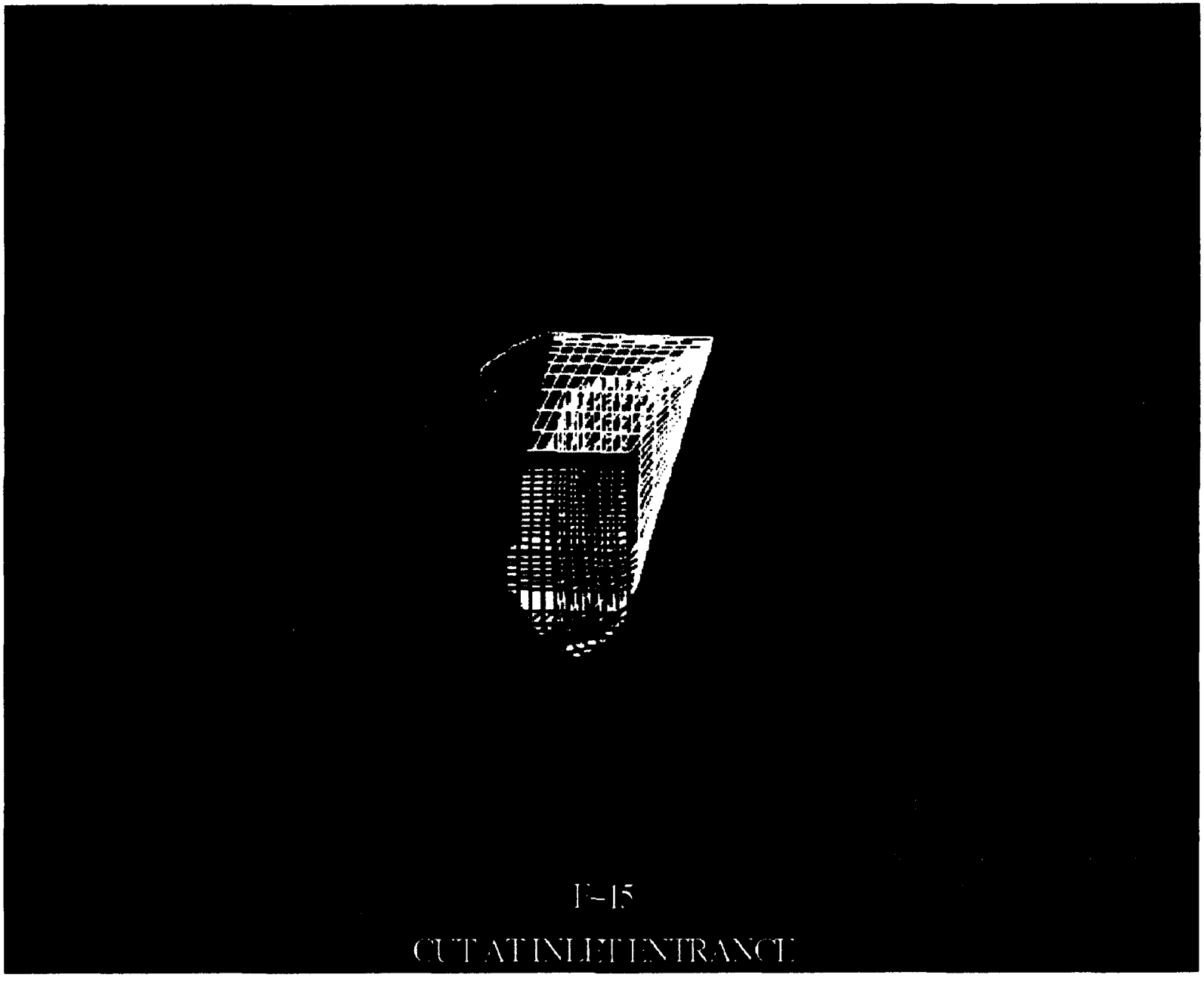

Figure 18. Grid Plane On Interior of Inlet to Allow for Flow-Through Calculations

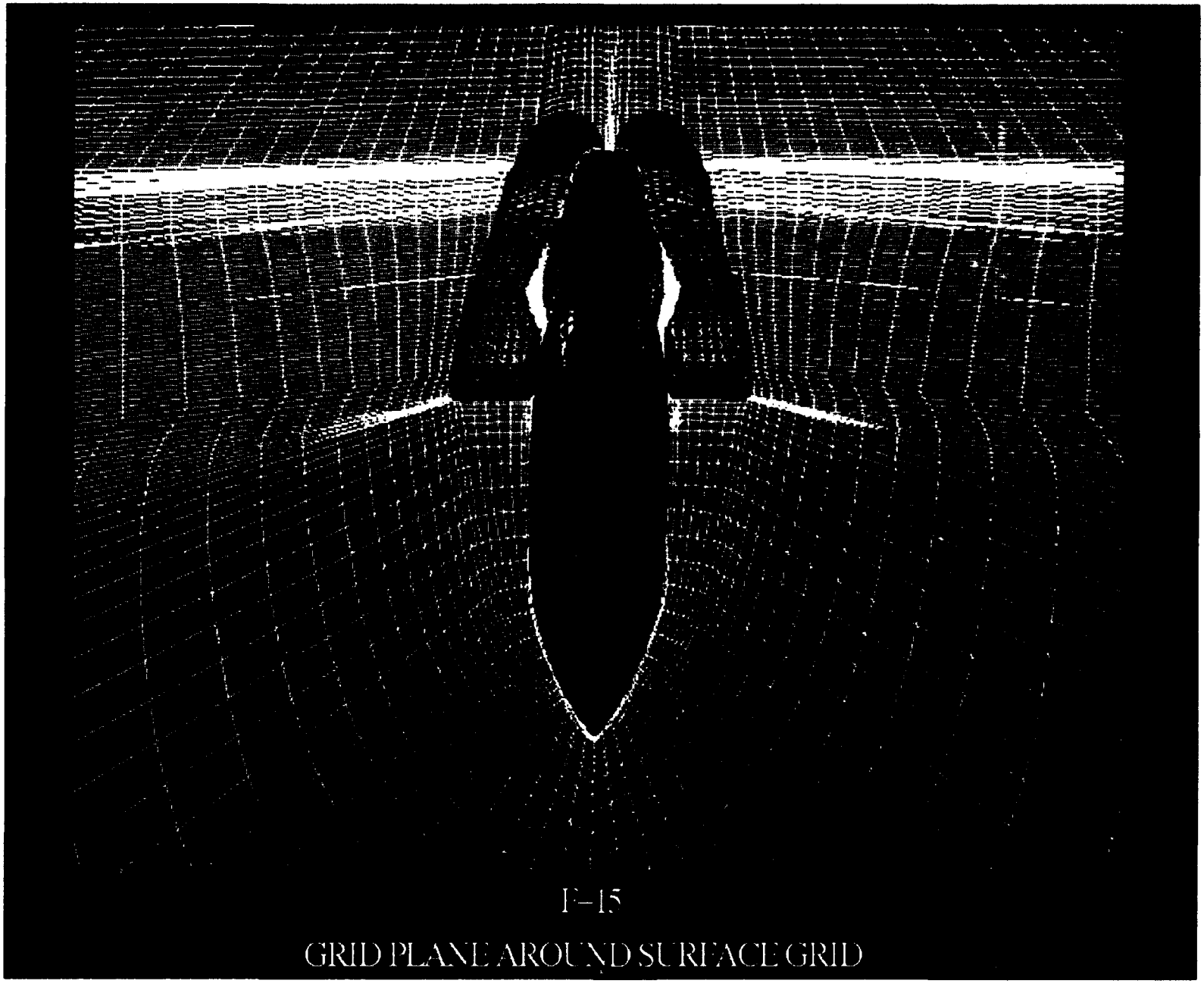

Figure 19. I-Constant Plane Depicting Grid Lines Entering Inlet

Figure 20. Proposed Zonal Grid Regions

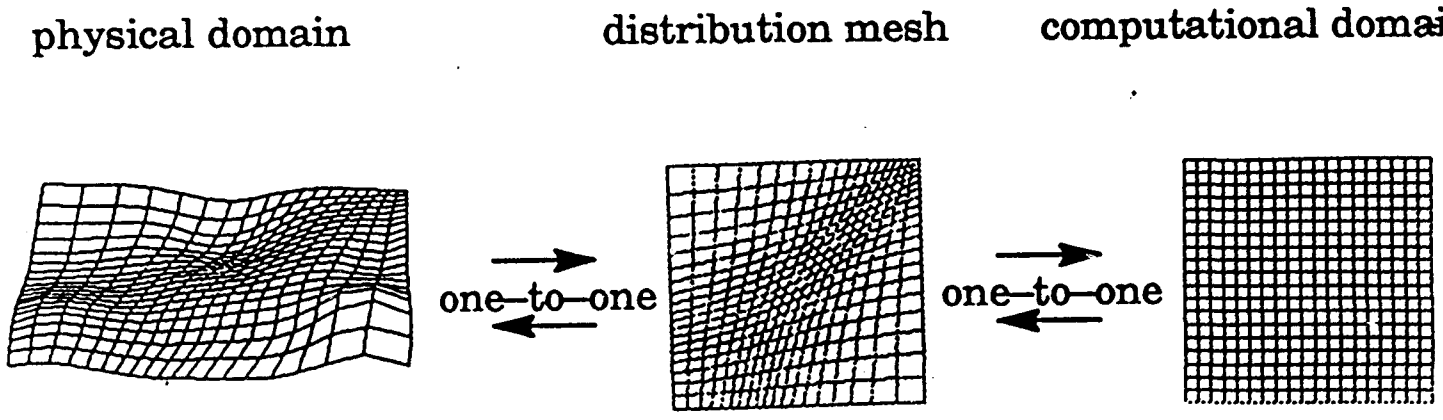

Figure 21. The one–to–one correspondence among physical domain, distribution mesh, and computational domain

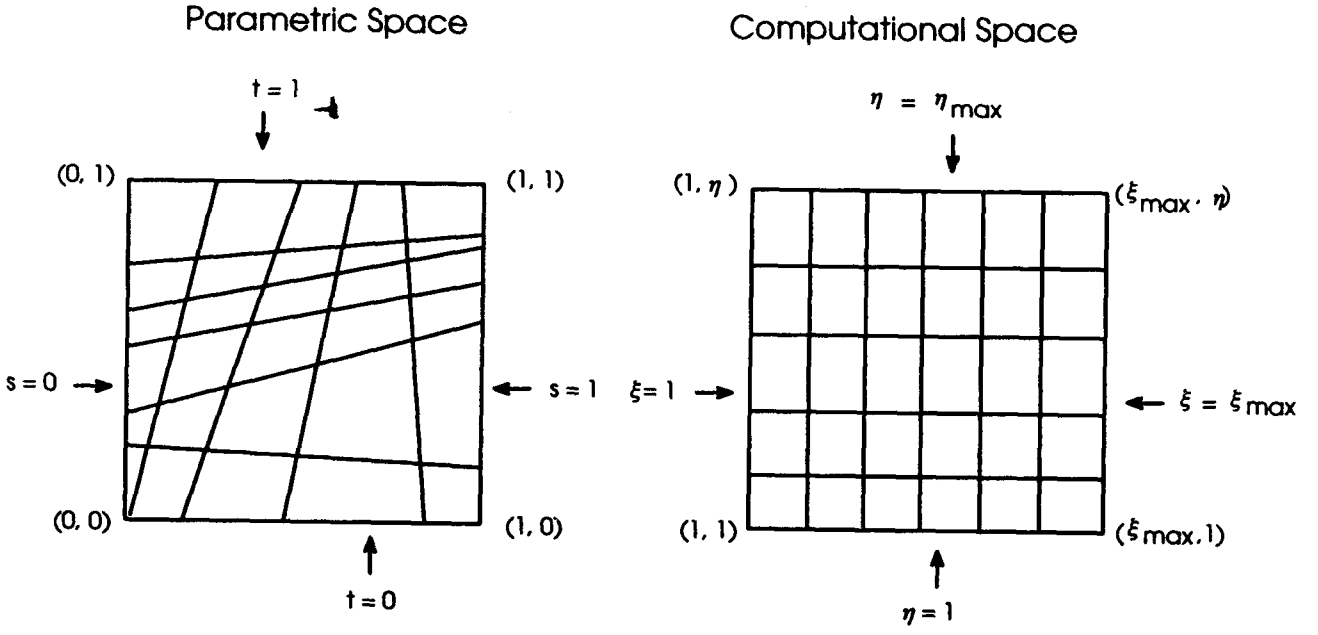
Parametric Space
Computational Space
t = 1
(0, 1)
(1, 1)
s = 0
s = 1
(0, 0)
(1, 0)
t = 0
η = ηmax
(1, η)
(ξmax, η)
ξ = 1
ξ = ξmax
(1, 1)
(ξmax, 1)
η = 1

Figure 22

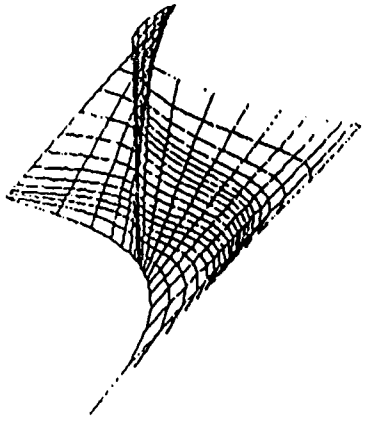

Figure 23a.
Original surface (view # 1)

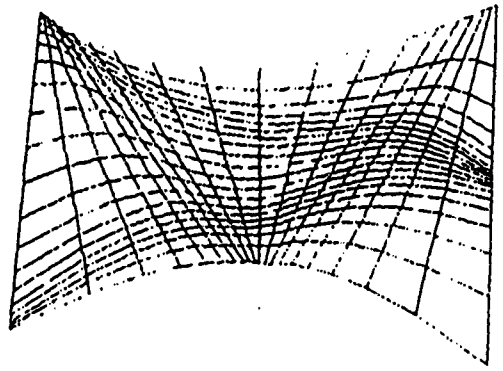

Figure 23b.
Original surface (view # 2)

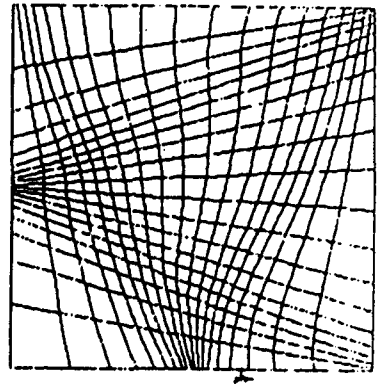

Figure 23e.
Parametric surface (original surface)

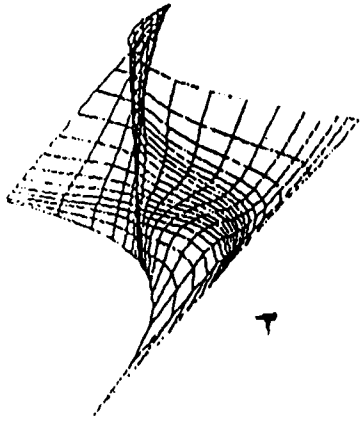

Figure 23c.
Optimized surface (view # 1)

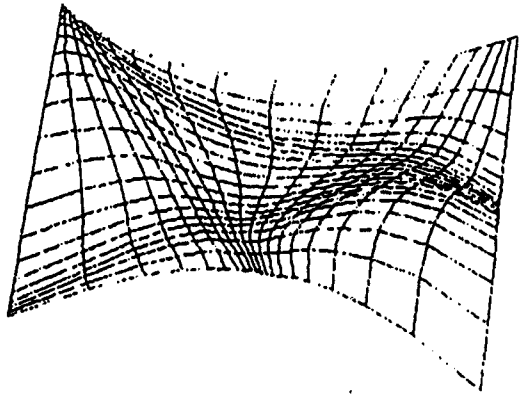

Figure 23d.
Optimized surface (view # 2)

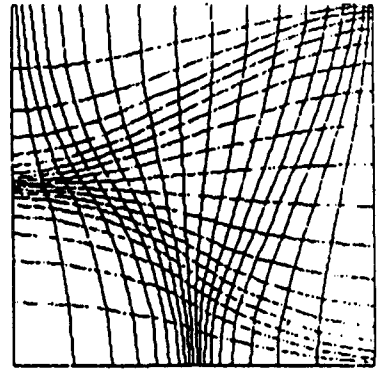

Figure 23f.
Optimized parametric surface

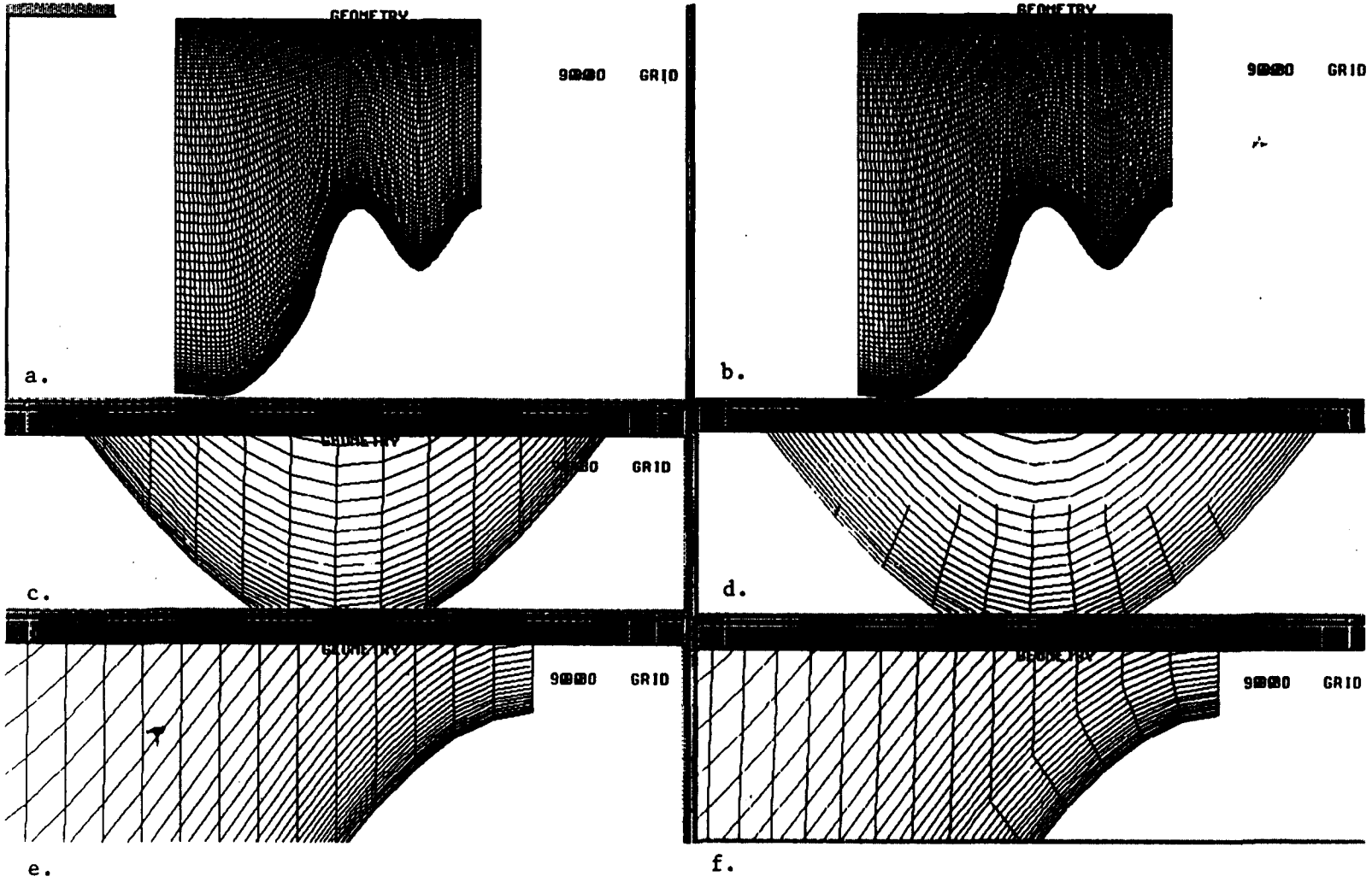

Algebraic Grid

Elliptic Grid

Figure 24. Arbitrary Configuration (with close-up grid views)

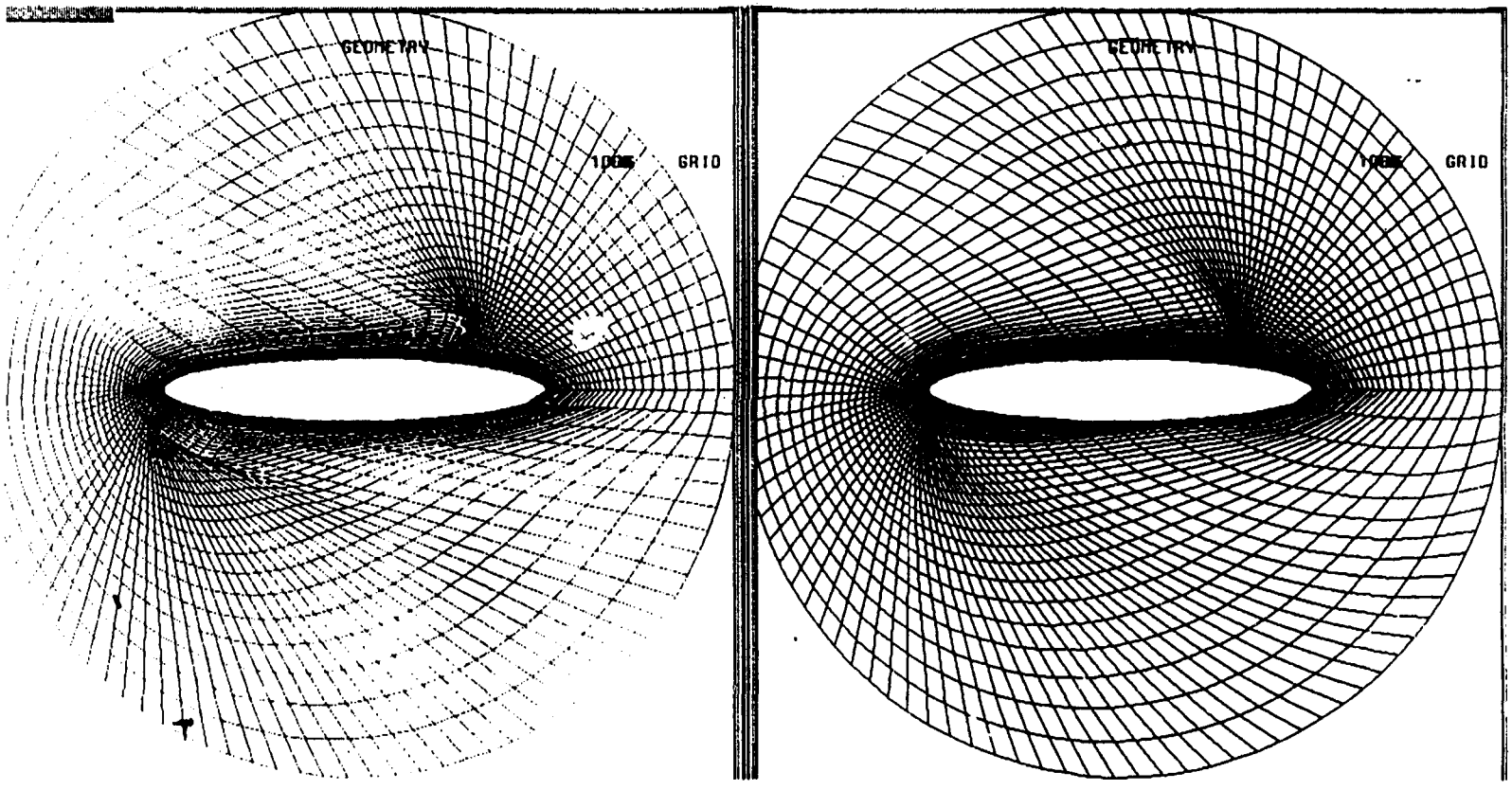

Figure 25a. Algebraic Grid

Figure 25b. Elliptic Grid

Figure 25. Airfoil Type Grid

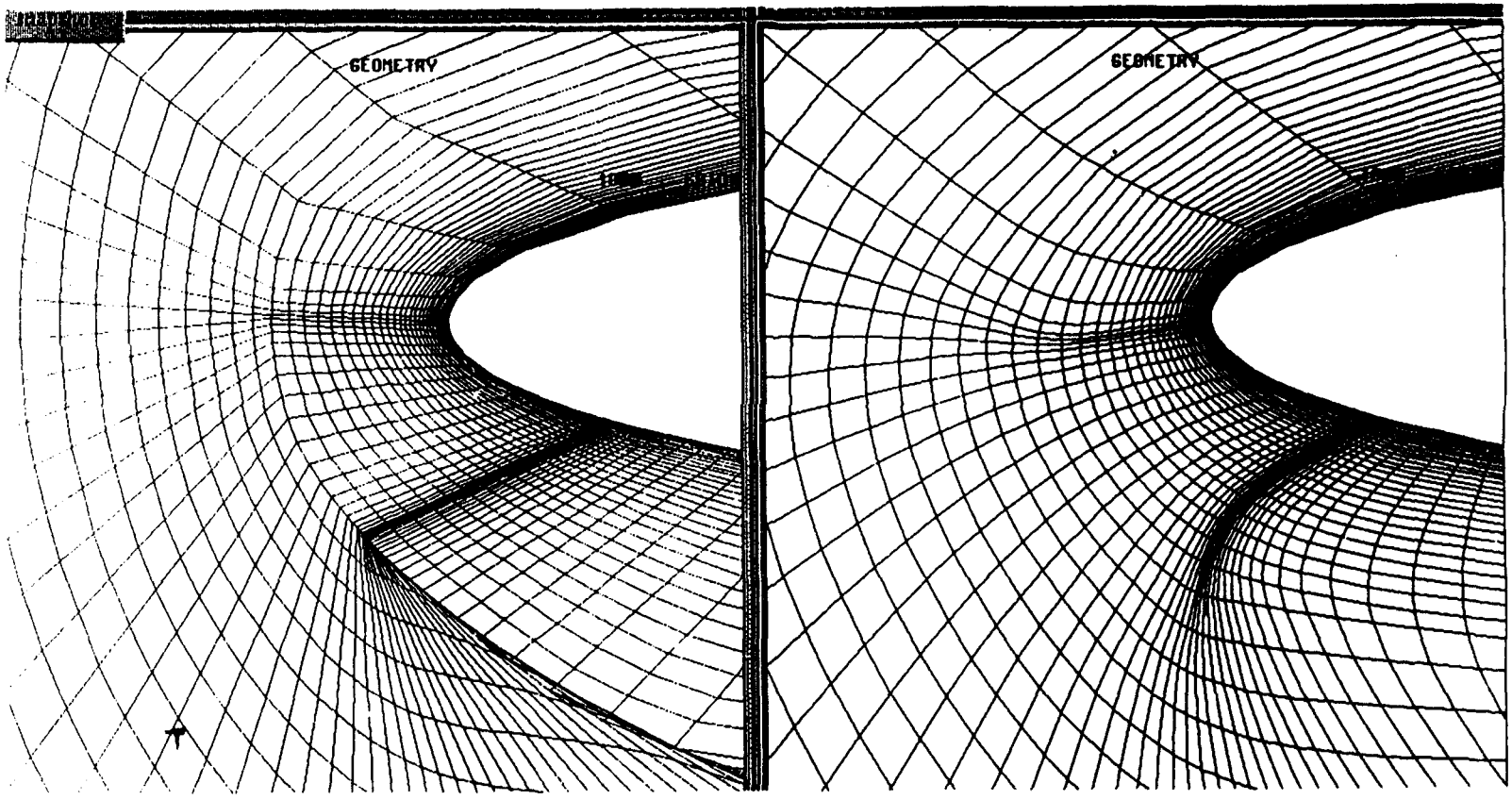

Figure 25c. Algebraic Grid

Figure 25d. Elliptic Grid

Figure 25. Magnified Grid near Skewed Cells

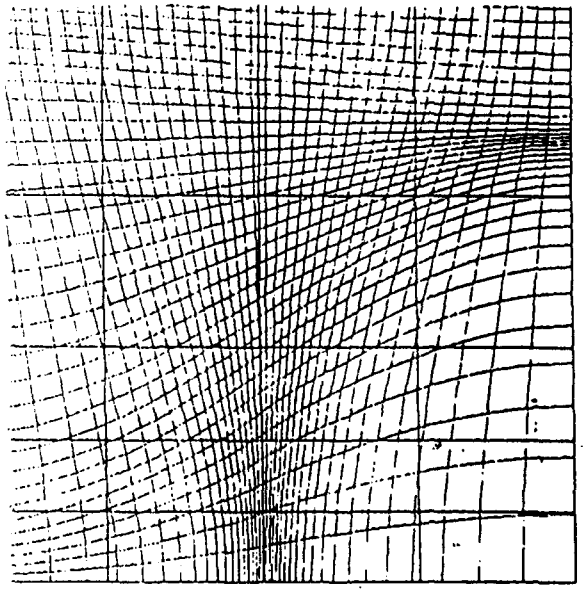

Figure 27a. Desired Parametric Space (Overlayed on Surface Definition Parametric Space)

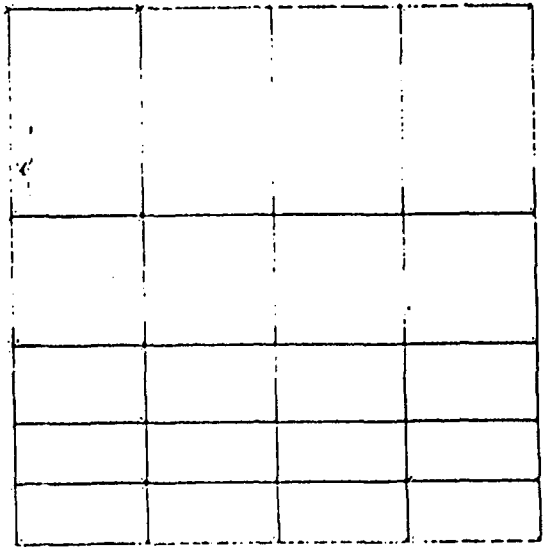

Figure 26b. Distribution (Parametric) Associated with Surface in 26a

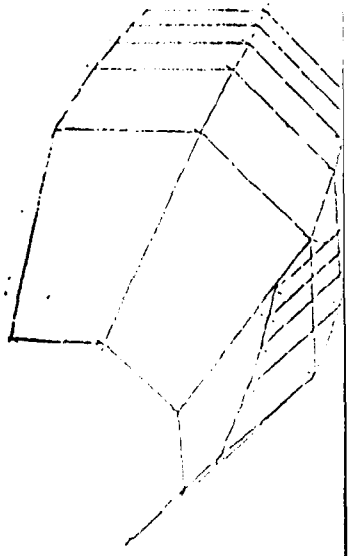

Figure 26a. Original Sculptured Surface

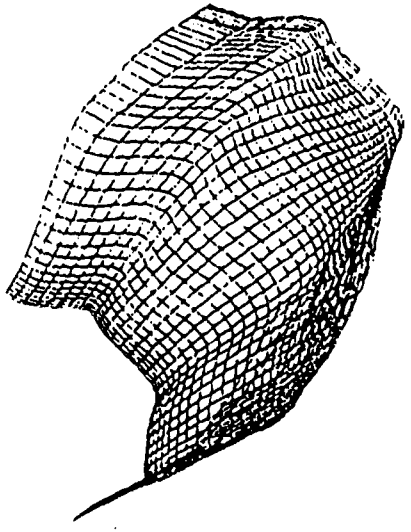

Figure 27b. Redistributed Surface Cubic Spline Definition

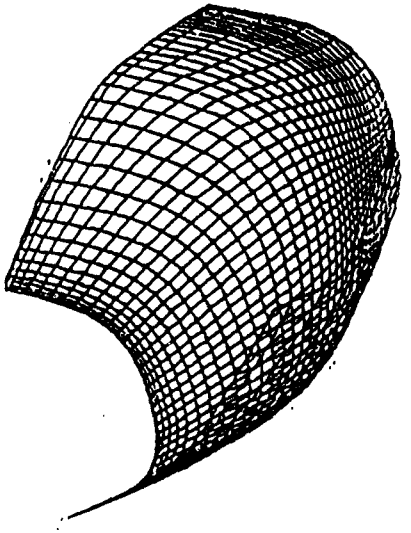

Figure 27c. Redistributed Surface Grid NURBS Definition

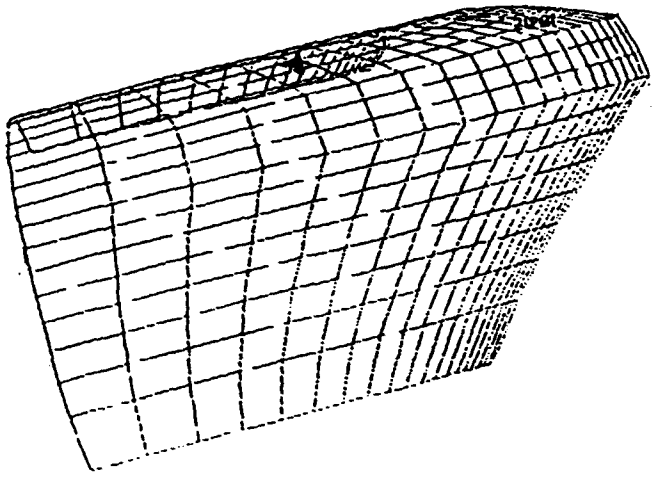

Figure 28a. C-Grid on A Surface

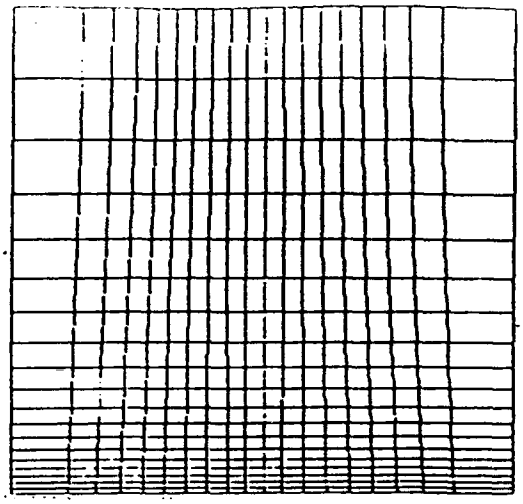

Figure 29a. Parametric Space Associated with C-Typed Grid

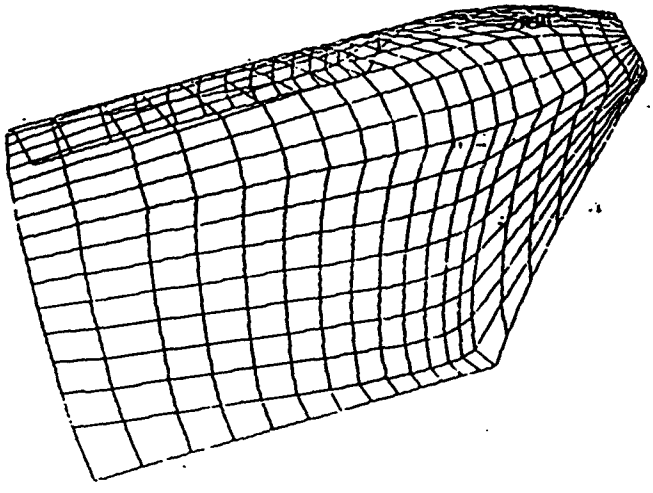

Figure 28b. Remapped O-Type Grid

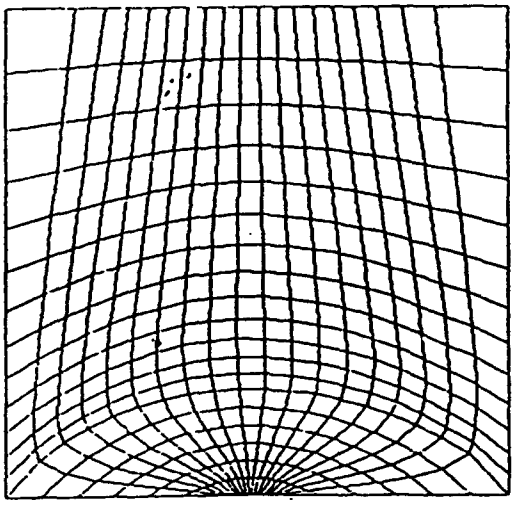

Figure 29b. Parametric Space for O-Type Grid

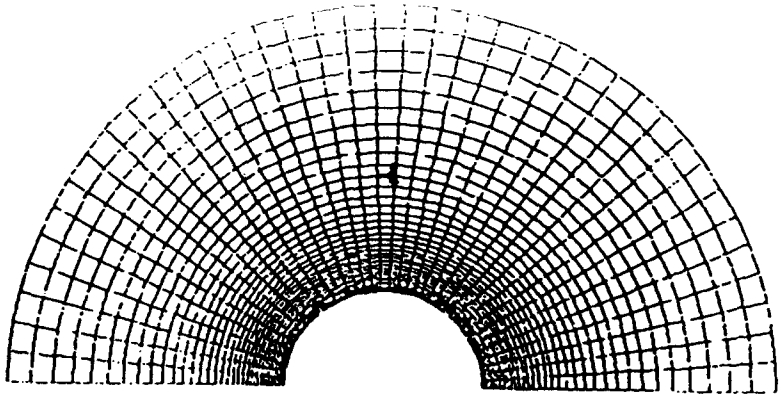

Figure 30a. Initial O-Type Grid

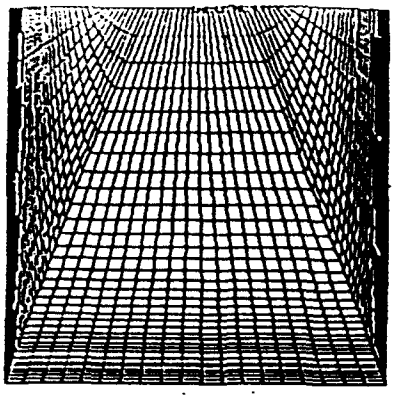

Figure 30c. Remapped Parametric Space for the desired H-Type Grid

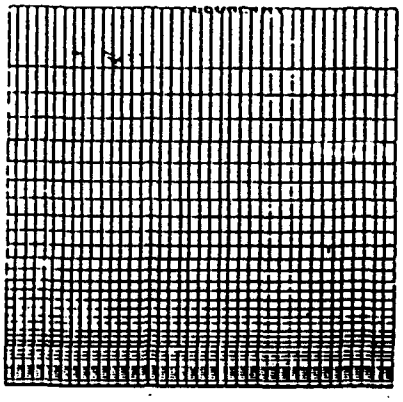

Figure 30b. Parametric Space Associated with Initial O-Type Grid

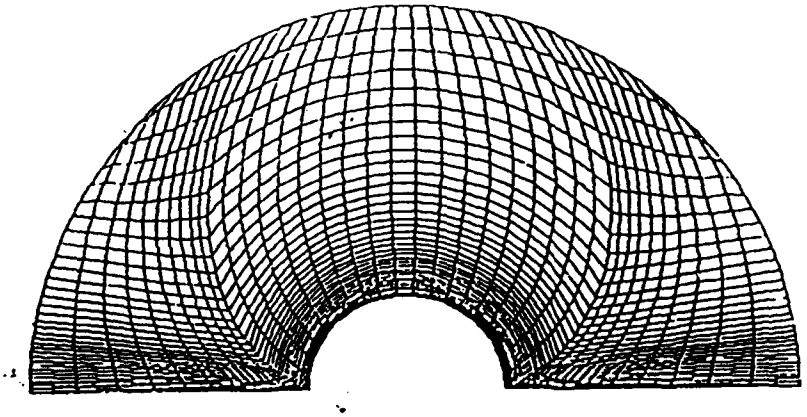

Figure 30d. Resulting H-Type Grid

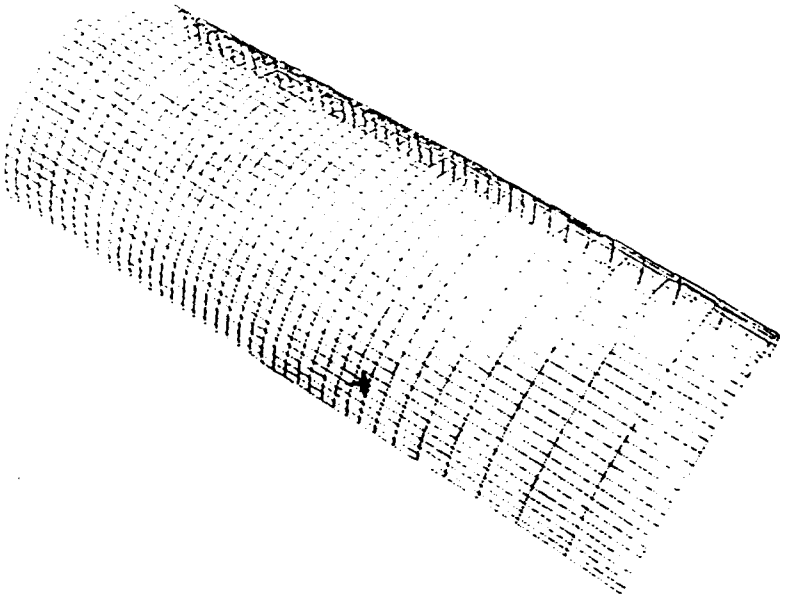

Figure 31a. Initial Surface Grid

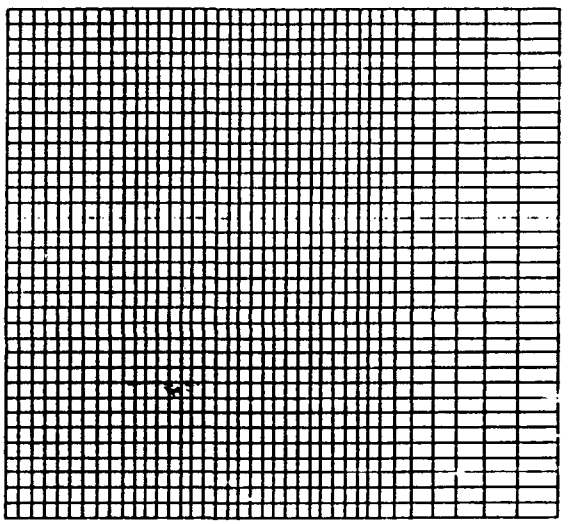

Figure 31b. Parametric Space Associated with the Initial Surface Grid

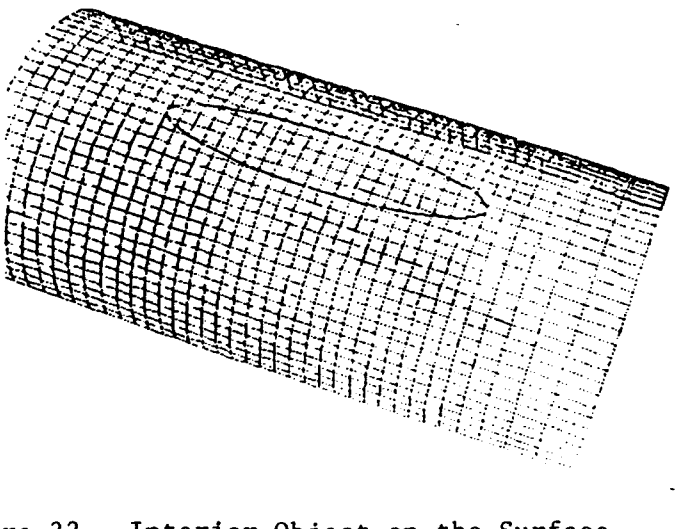

Figure 32. Interior Object on the Surface

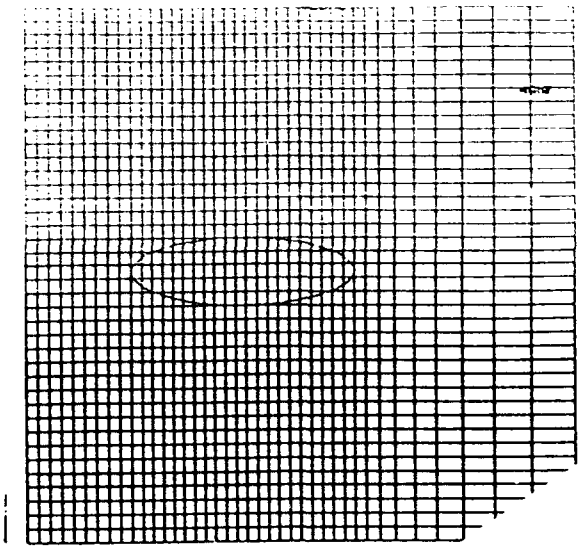

Figure 33. Parametric Values for Initial Surface and the Interior Object

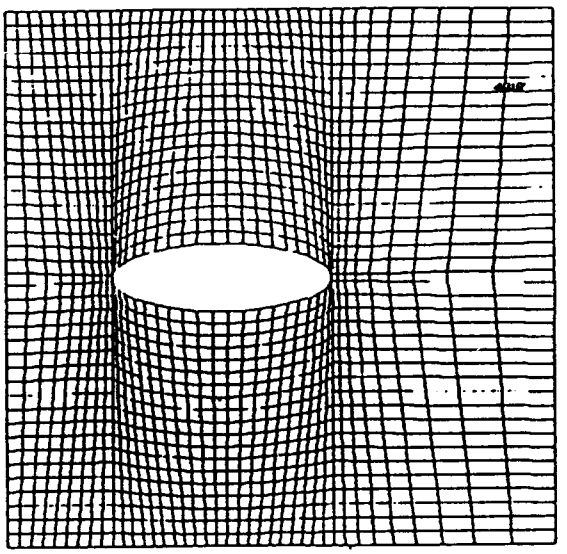

Figure 34. Reparameterized Distribution Space

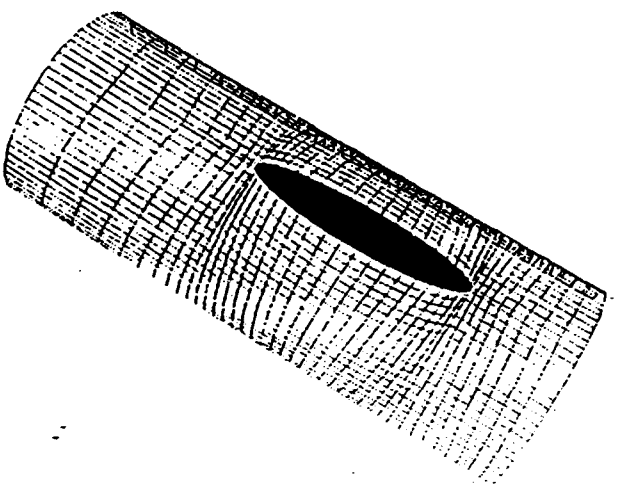

Figure 35. Resulting Surface Grid

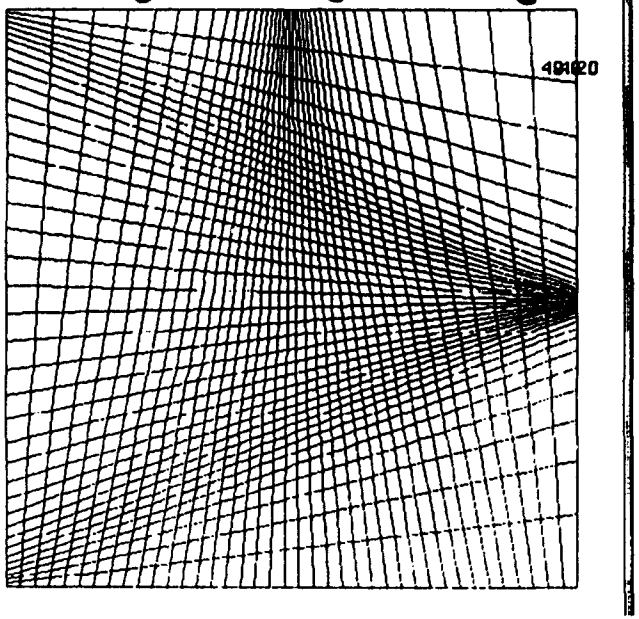

Figure 36a. Algebraic Grid

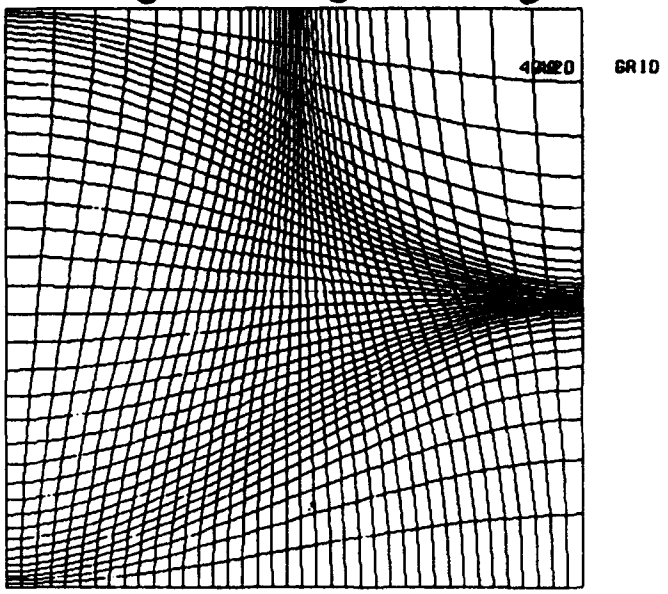

Figure 36b. Optimized Grid

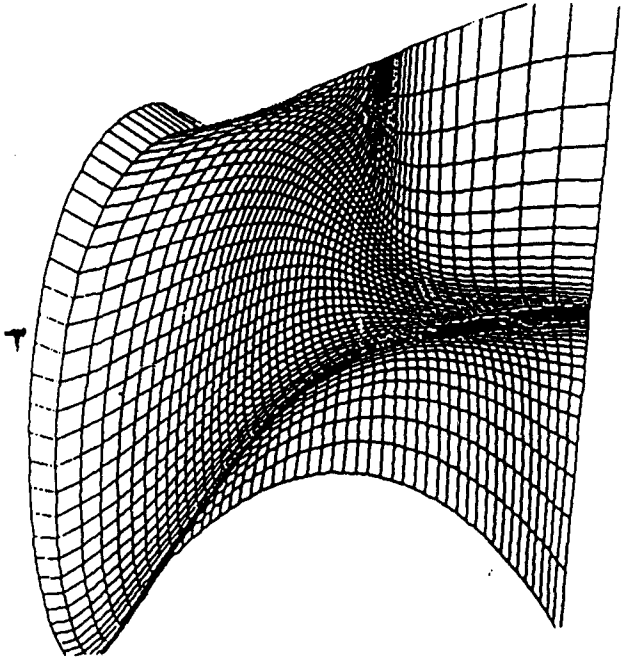

Figure 36c. Algebraic Grid

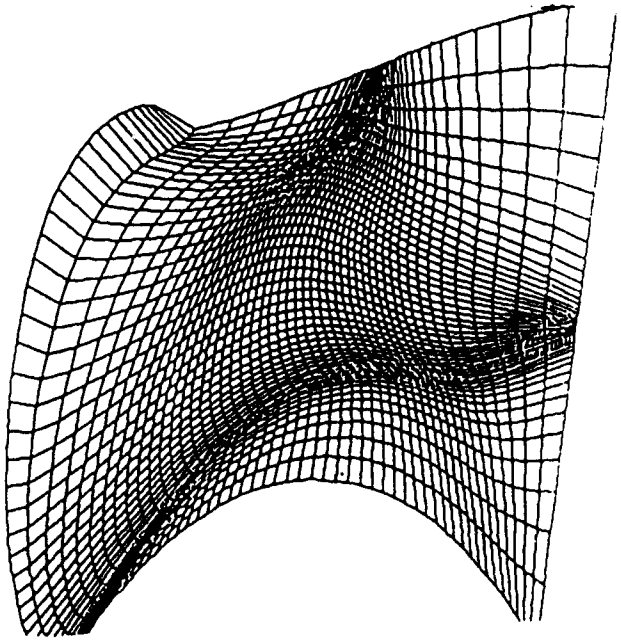

Figure 36d. Optimized Grid

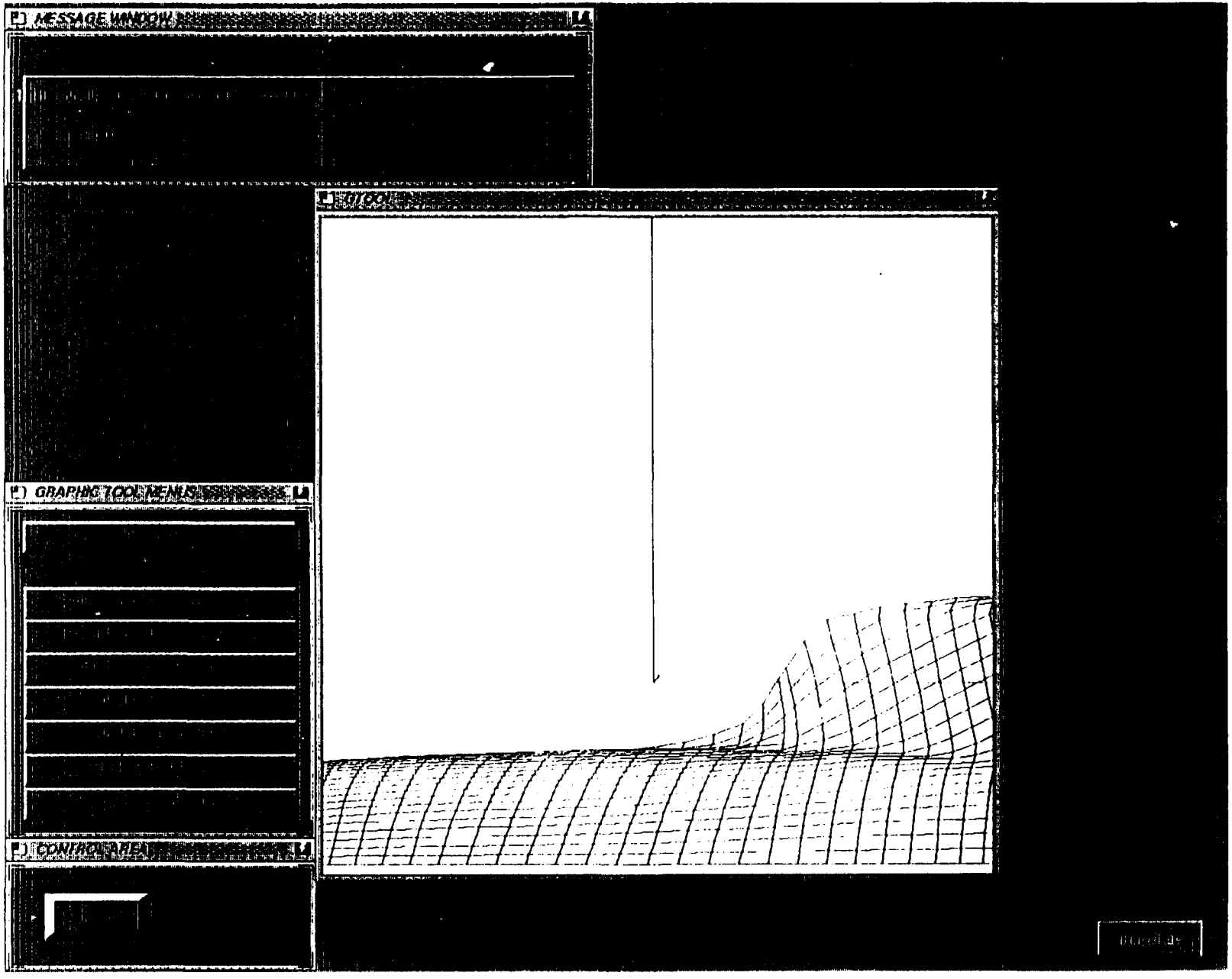

Figure 37. Characteristic Analysis: Angle Checking - Display

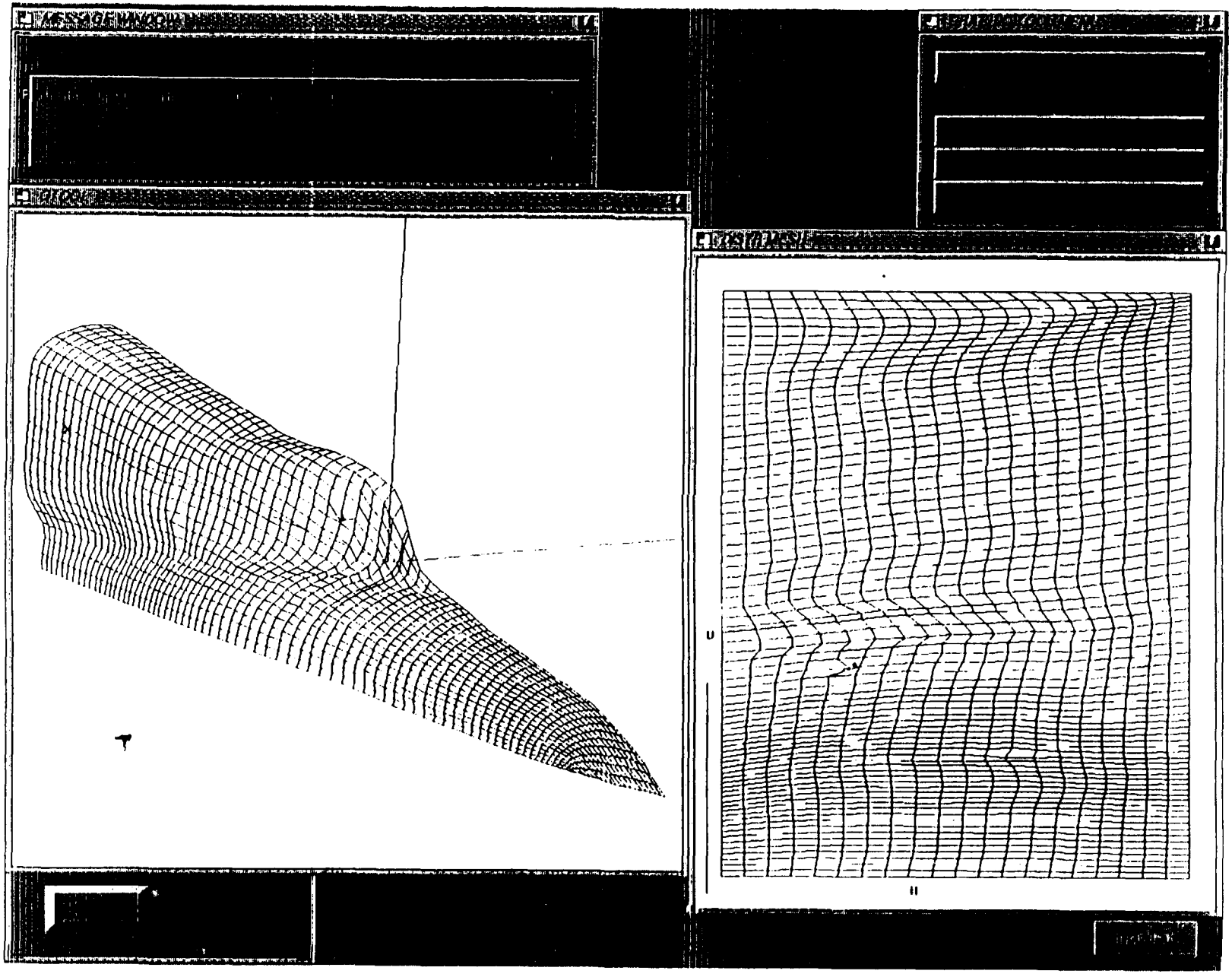

Figure 38a. Physical Surface Grid

Figure 38b. Surface Parametric Space

Figure 38. Characteristic Analysis: Surface Manipulation

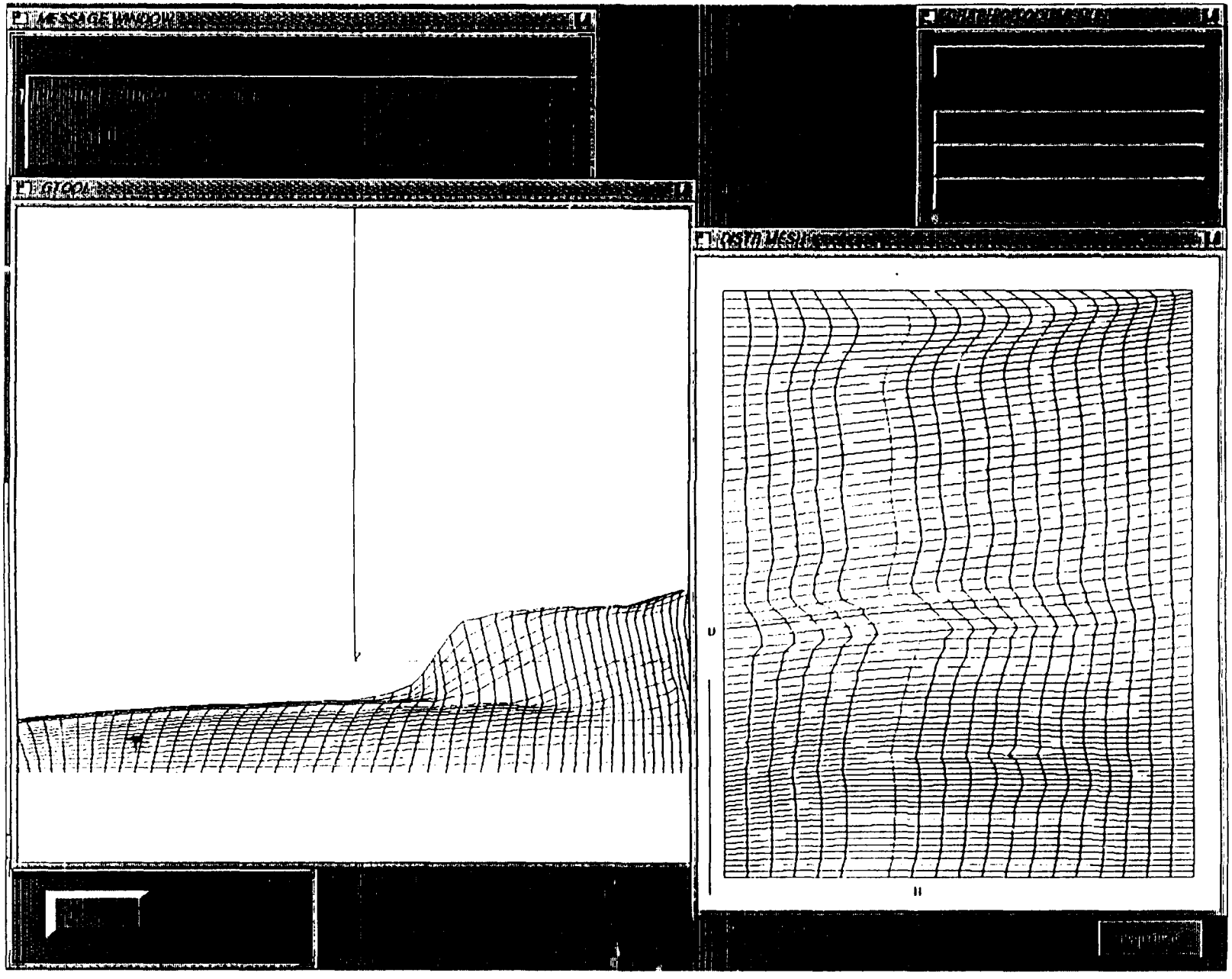

Figure 39a. Physical Surface Grid

Figure 39b. Surface Parametric Space

Figure 39. Characteristic Analysis: Surface Manipulation (Line Removal)

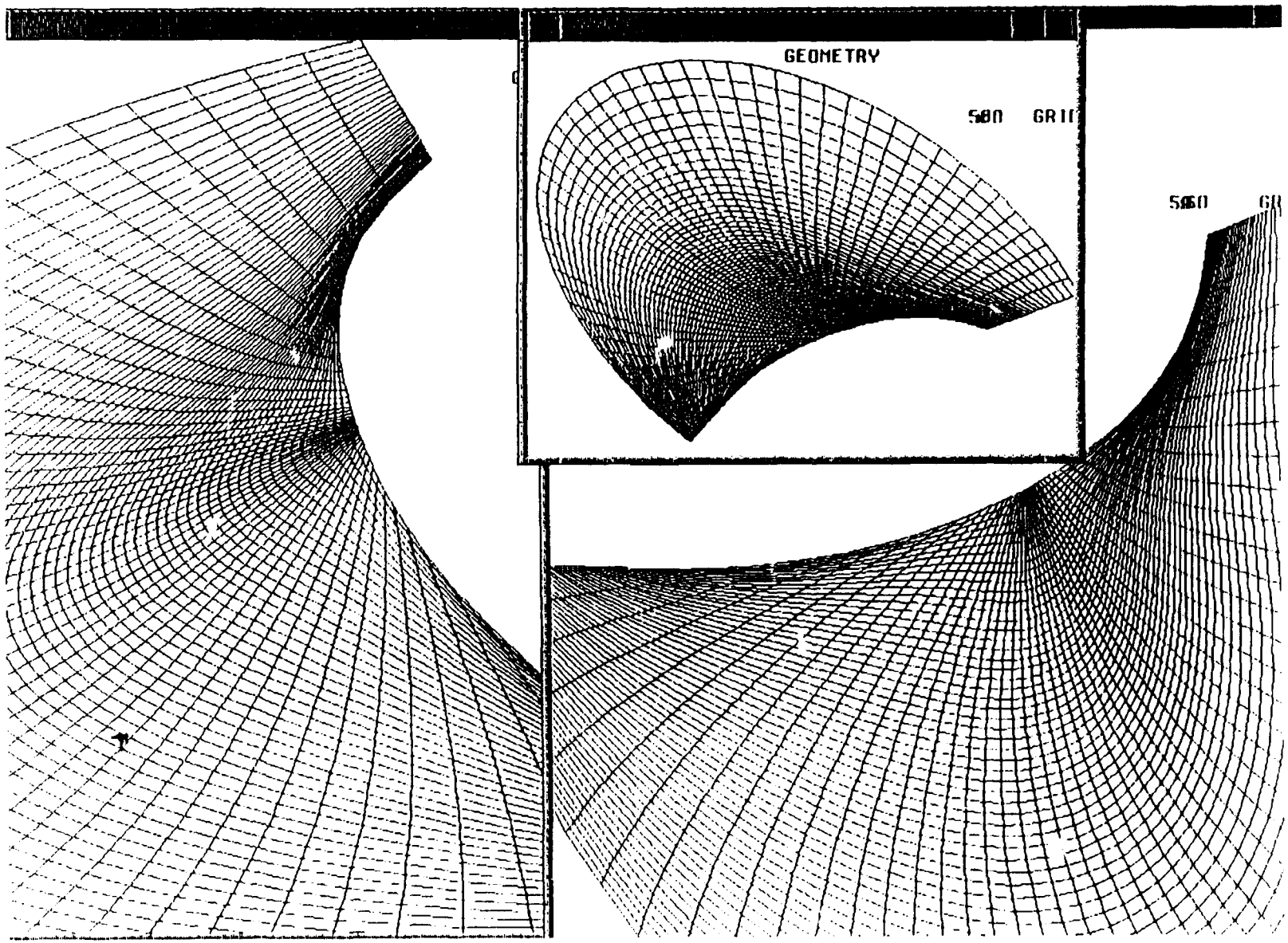

Figure 40. Crossing Check (60 x 50 Size) Surface Grid Display

```
crossing  1  at i=  1 j=  1
crossing  2  at i=  1 j=  2
crossing  3  at i=  1 j=  3
crossing  4  at i=  1 j=  4
crossing  5  at i=  1 j=  5
crossing  6  at i=  1 j=  6
crossing  7  at i=  1 j=  7
crossing  8  at i=  1 j=  8
crossing  9  at i=  1 j=  9
crossing 10  at i=  1 j= 10
crossing 11  at i=  1 j= 11
crossing 12  at i=  1 j= 12
crossing 13  at i=  2 j=  7
crossing 14  at i=  2 j=  8
crossing 15  at i=  2 j=  9
crossing 16  at i=  2 j= 10
crossing 17  at i=  2 j= 11
crossing 18  at i=  2 j= 12
crossing 19  at i=  2 j= 13
crossing 20  at i=  3 j=  1
crossing 21  at i=  3 j=  2
crossing 22  at i=  3 j=  3
crossing 23  at i=  3 j=  4
crossing 24  at i=  3 j=  5
crossing 25  at i=  3 j=  6
crossing 26  at i=  3 j=  7
crossing 27  at i=  3 j=  8
crossing 28  at i= 48 j=  1
crossing 29  at i= 48 j=  2
crossing 30  at i= 49 j=  4
crossing 31  at i= 49 j=  5
crossing 32  at i= 49 j=  6
crossing 33  at i= 49 j=  7
crossing 34  at i= 49 j=  8
```

Maximum Area 0.027 275 at i = 43 j = 39

Minimum Area 0.00025 at i = 3 j = 8

Figure 41. Listing of Crossings Found

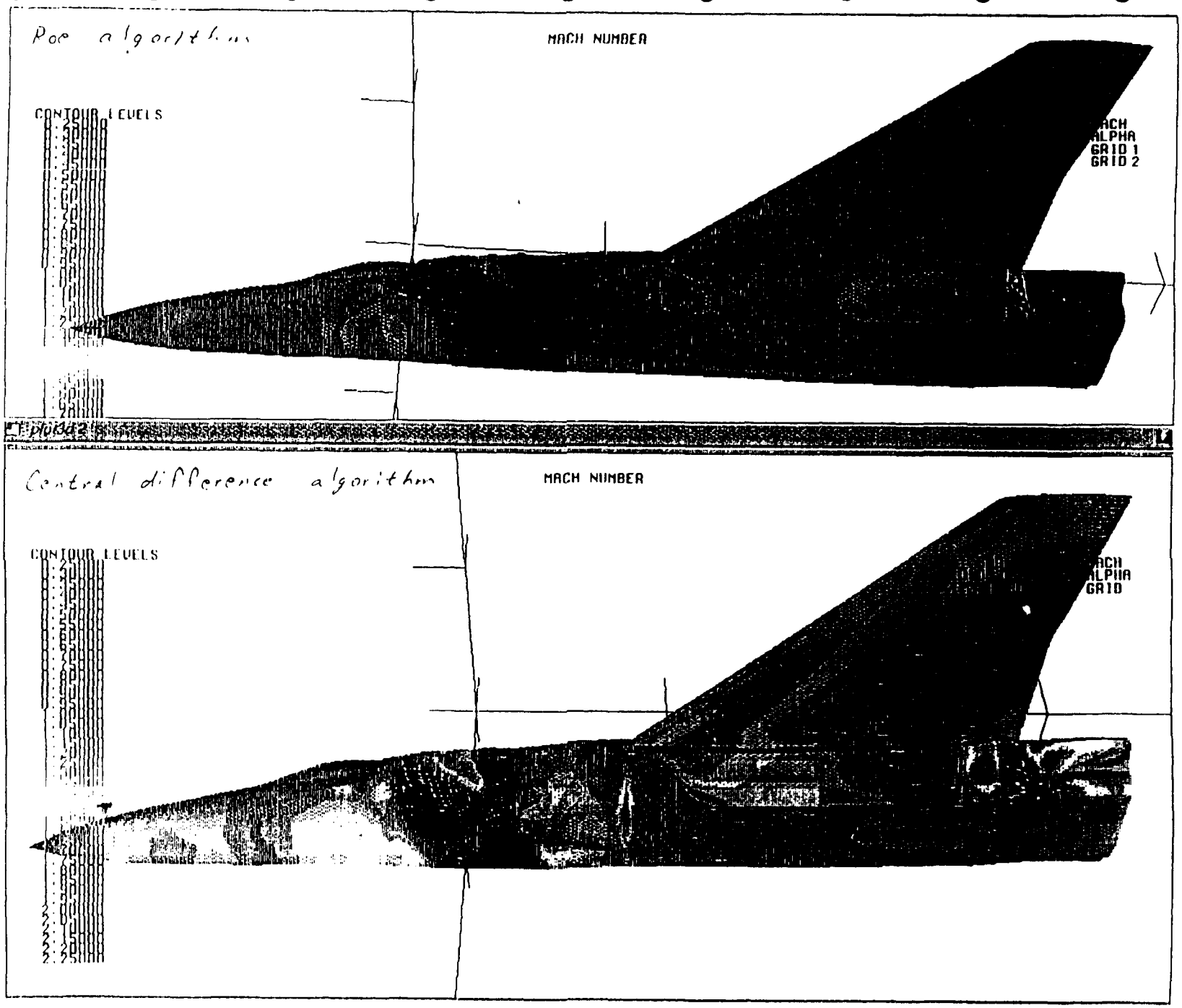

Figure 42. Surface Mach Number Comparison Between Roe Algorithm and Central Difference Algorithm

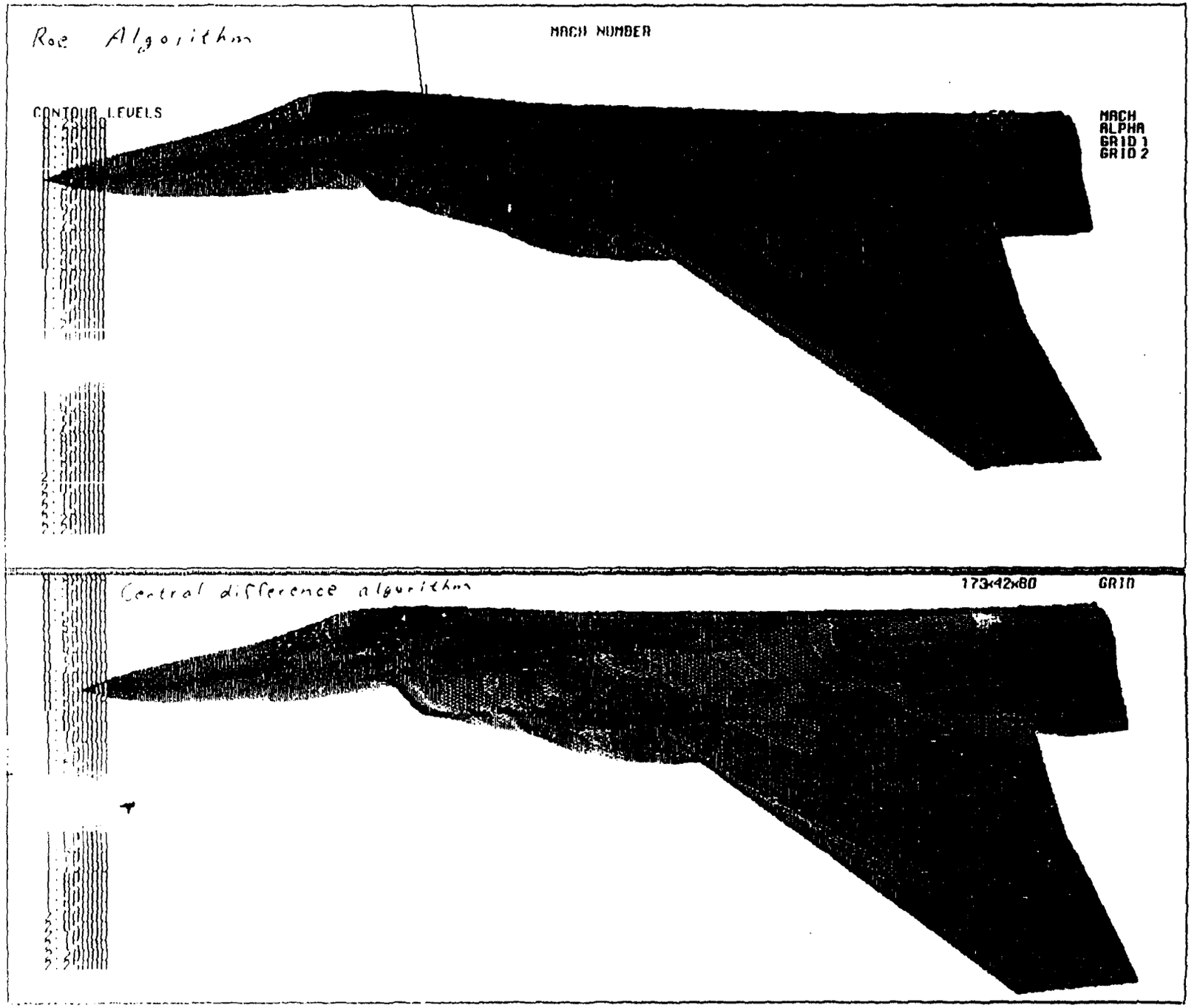

Figure 43. Surface Mach Number Comparison Between Roe Algorithm and Central Difference Algorithm

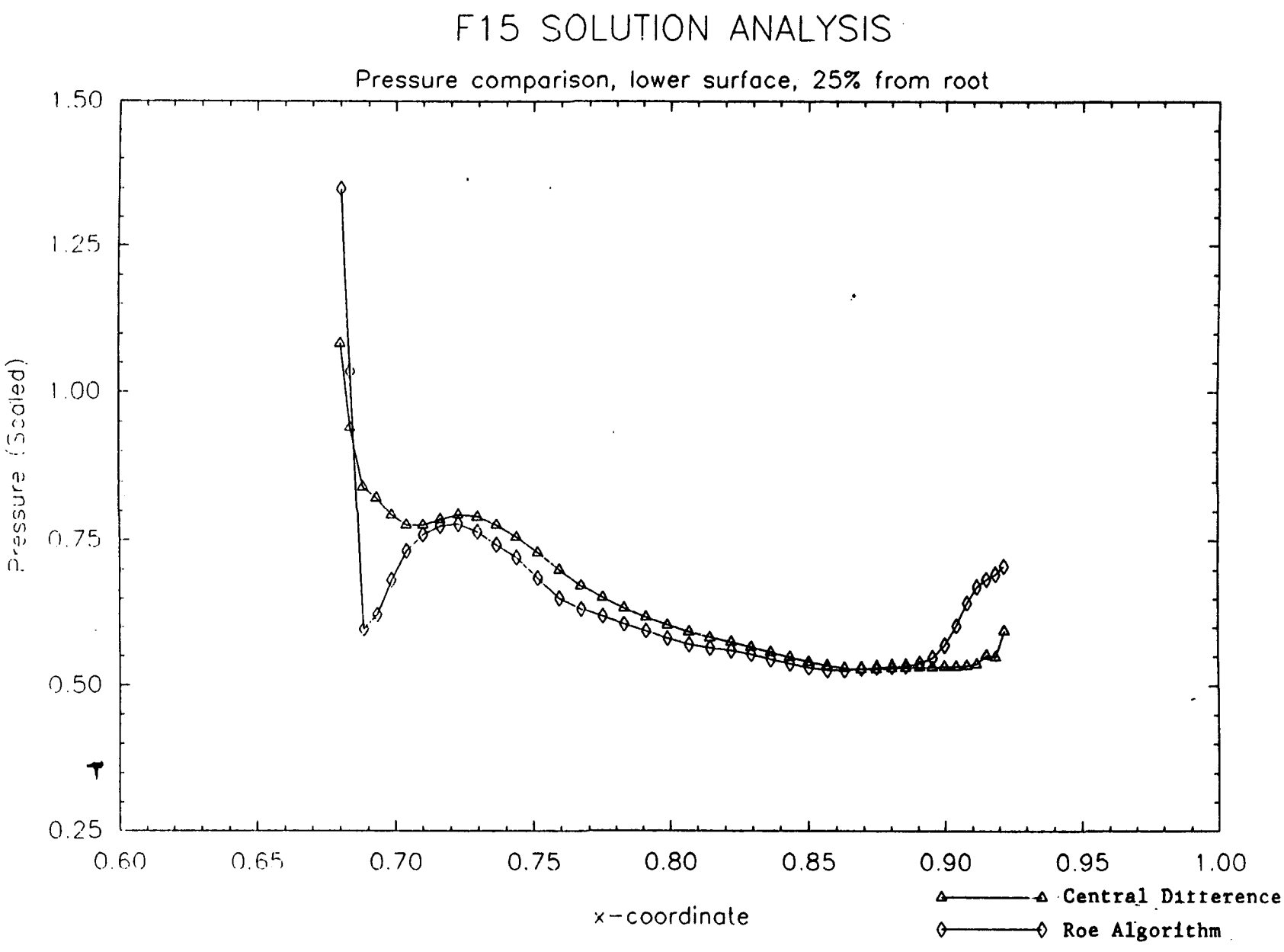

Figure 44. Pressure Comparison on Lower Wing Surface, 25% from Root

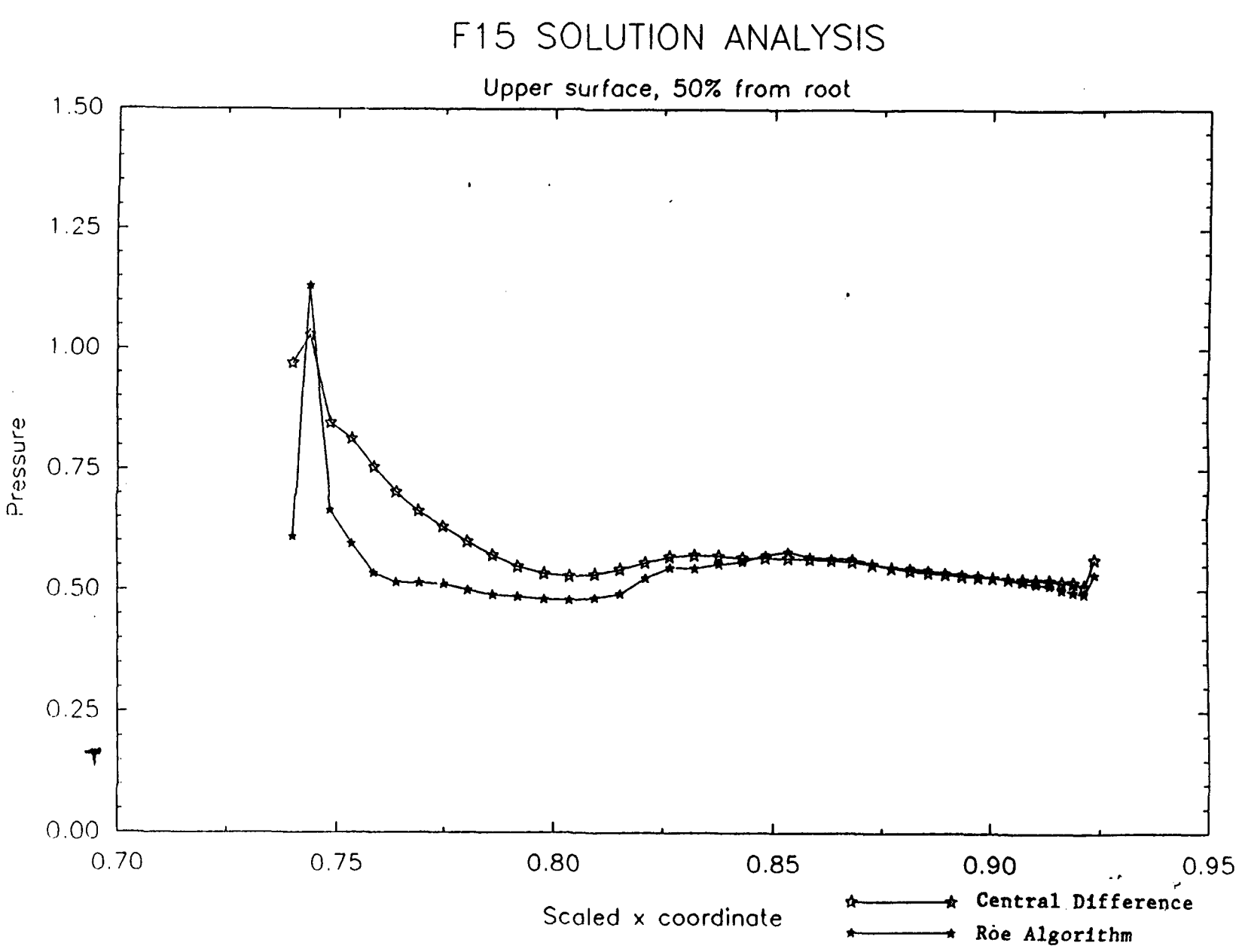

Figure 45. Pressure Comparison on Upper Wing Surface, 50% from Root

Pressure on F-15 Body

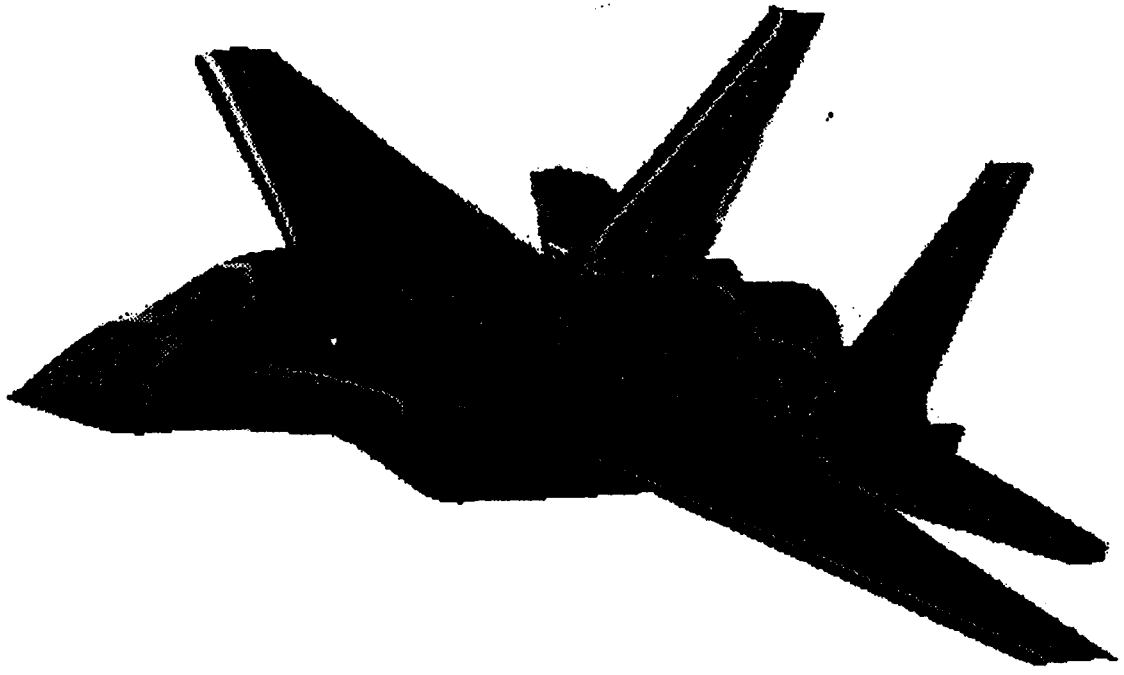

Figure 46. Surface Pressure - Parallel Computation